Projections of future water resources and their uncertainty in a glacierized catchment in the Swiss Alps and the subsequent effects on hydropower production during the 21st century

David Finger,[1,2] Georg Heinrich,[3] Andreas Gobiet,[3] and Andreas Bauder[4]

Received 31 March 2011; revised 29 December 2011; accepted 5 January 2012; published 18 February 2012.

[1] Hydropower accounts for about 20% of the worldwide electrical power production. In mountainous regions this ratio is significantly higher. In this study we present how future projected climatic forcing, as described in regional climate models (RCMs), will affect water resources and subsequently hydropower production in downstream hydropower plants in a glacierized alpine valley (Vispa valley, Switzerland, 778 km^2). In order to estimate future runoff generation and hydropower production, we used error-corrected and downscaled climate scenarios from regional climate models (RCMs) as well as glacier retreat projections from a dynamic glacier model and coupled them to a physically based hydrological model. Furthermore, we implemented all relevant hydropower operational rules in the hydrological model to estimate future hydropower production based on the runoff projections. The uncertainty of each modeling component (climate projections, glacier retreat, and hydrological projection) and the resulting propagation of uncertainty to the projected future water availability for energy production were assessed using an analysis of variance. While the uncertainty of the projections is considerable, the consistent trends observed in all projections indicate significant changes to the current situation. The model results indicate that future melt- and rainfall-runoff will increase during spring but decline during summer. The study concludes by outlining the most relevant expected changes for hydropower operations.

Citation: Finger, D., G. Heinrich, A. Gobiet, and A. Bauder (2012), Projections of future water resources and their uncertainty in a glacierized catchment in the Swiss Alps and the subsequent effects on hydropower production during the 21st century, *Water Resour. Res.*, *48*, W02521, doi:10.1029/2011WR010733.

1. Introduction

[2] Although about 20% of the gross electricity production worldwide comes from hydropower plants, the economic potential of hydropower has not been exploited completely [*Sternberg*, 2010]. In mountainous regions, the ratio of hydropower production is significantly higher, e.g., in Austria and Switzerland hydropower accounts for more than 50% of the national electrical power production [*Zimmermann*, 2001]. In these countries, the hydropower potential is nearly exploited completely or will not be further developed for various environmental reasons [*Finger et al.*, 2006; 2007; *Jager and Smith*, 2008; *Miranda*, 2001]. In particular, reservoirs are important constituents of power production, as they can react to the electricity consumption variations within seconds and thus ensure sufficient energy supply for adequate network stability. Nevertheless, hydropower production depends on local precipitation, snow coverage, and glacier ice melting, and is therefore subject to important interannual fluctuations [*Bartolini et al.*, 2009; *Lambrecht and Mayer*, 2009].

[3] Throughout the last century hydropower plants have been adapted and improved to optimize power production and other services [*Alfieri et al.*, 2006; *Egre and Milewski*, 2002]. Nevertheless, climate change remains one of the biggest challenges for the hydropower sector [*Lehner et al.*, 2005], in particular in Switzerland, where reservoirs are frequently glacier fed [*Hauenstein*, 2005]. Water resources in mountain regions are particularly sensitive to climatic forcing as glacier retreat is already affecting hydropower production across the Alps [*Hock*, 2005]. Although increasing water runoff has been observed in many mountain streams below glaciers in recent years, discharge is expected to decrease in the future, when glaciers will have shrunk below a threshold extent [*Huss*, 2011; *Huss et al.*, 2008; *Stahl and Moore*, 2006]. According to the IPCC report [*IPCC*, 2008], the hydropower potential is expected to decline by 6%, with strong regional variations from a 20%–50% decrease in the Mediterranean region to a 15%–30% increase in Northern and Eastern Europe. These predictions will doubtlessly affect energy production and flood control, so that water management measures will have to be adapted accordingly [*Xu and Singh*, 2004].

[1] Institute of Environmental Engineering, ETH Zurich, Switzerland.
[2] Now at Institute of Geography and Oeschger Centre for Climate Change Research, University of Bern, Bern, Switzerland.
[3] Wegener Center for Climate and Global Change (WEGC) and Institute for Geophysics, Astrophysics, and Meteorology/Inst. of Physics (IGAM/IP), University of Graz, Graz, Austria.
[4] Laboratory of Hydraulics, Hydrology and Glaciology (VAW), ETH Zurich, Switzerland.

0043-1397/12/2011WR010733

*Errors to the author affiliations were introduced during the production of this article. The PDF version is correct here. The article as originally published appears in the HTML.

[4] In Switzerland the *Federal Office of Energy* (SFOE) estimates that in the long term 2000 hydro GWh a^{-1} will be lost due to climate change and 1900 GWh a^{-1} due to legal residual water flows [*OFEN*, 2004]. Such estimations rely, however, on empirical linear projections and provide only limited information for future water management strategies. Projections performed with hydrological models, using state of the art climate projections, can help in developing adequate water management strategies to anticipate expected changes. Efforts to assess such changes have been made by *Mimikou and Baltas* [1997] using three global circulation model (GCM) outputs to evaluate the reliability of a hydropower scheme, by *Bergström et al.* [2001] to assess the potential of future power plants in Sweden, and several authors in the western United States have used different GCM and downscaling techniques to assess future water resources [*Christensen et al.*, 2004; *Payne et al.*, 2004], to name just a few. While the use of different climate scenarios reveals the uncertainty of climate projections, it is also essential to quantify and discuss the uncertainty propagated to the future hydrological projections. For example, *Minville et al.* [2008] and *Kay et al.* [2009] investigated different sources of uncertainty and demonstrated that the uncertainty of future hydrological projections is primarily due to uncertainties within the choice of a global climate model (GCM). *Schäfli et al.* [2007] were the first to present a thorough approach to compare modeling uncertainties with projected changes due to climate change for a small case study in Switzerland. *Stahl et al.* [2008] incorporated periodic changes in glacier cover in a conceptual model to project future runoff generation. However, all these previous studies do not account for dynamic glacier retreat and hydropower operational rules simultaneously, nor do they employ the newest state of the art error-corrected and downscaled climate scenarios. This makes their result less reliable and their modeling approaches can only be applied to study sites without river diversion. Furthermore, the propagation of the specific uncertainty from climate models and dynamic glacier models to final projections of future water resources has never been quantified.

[5] Motivated by the ongoing discussion about the impacts of climate change and its uncertainty on hydropower production [*SGHL*, 2011], our study presents an integrative modeling chain in which we couple error-corrected and downscaled scenarios from regional climate models (RCMs), glacier retreat from a dynamic glacier model, and a hydrological model which accounts for hydropower operational rules. For this purpose we integrated all relevant hydropower operational rules (diversion of mountain stream, storage in reservoirs, and routing of pressurized water to the turbines) in a physically based, fully distributed hydrological model and coupled the model to a dynamic glacier model and seven error-corrected and downscaled A1B forced RCM climate scenarios. This modeling chain allows us to investigate the impacts of climate change on complex hydropower installations which collect and divert water from several subcatchments with different degrees of glaciation.

[6] Furthermore, we quantify the uncertainties of climate change projections by assessing the variability in an ensemble of realistic projections of each modeling component. Subsequently, the propagation of the variability of each modeling component to the global uncertainty of projected runoff and hydropower production was assessed using an analysis of variance (ANOVA analysis). This approach allows us not only to quantify the uncertainty of our projections, but also to determine which modeling component is responsible for the uncertainty. Finally, we compare the projected changes in water availability with the expected natural variability of the annual cycle. This allows us to identify which projected changes are statistically stronger than the natural variability of future climate patterns. This identification is a prerequisite for establishing adequate water management policies for future periods.

[7] We chose the Vispa valley, a mountain valley in the Swiss Alps, for this study as its setting with two hydropower companies exploiting the natural runoff using complex operational rules is representative for typical modern hydropower storage plants. The study concludes by assessing the projected impact and its uncertainty of climatic change on future water resources and energy production in the valley. Our approach opens new possibilities to water resources managers to develop specific strategies to anticipate climate change impacts on hydropower production.

2. Study Site and Data

[8] The Vispa River is situated about 200 km east of Geneva (7° 50′ E, 46° 08′ N) in the southern part of

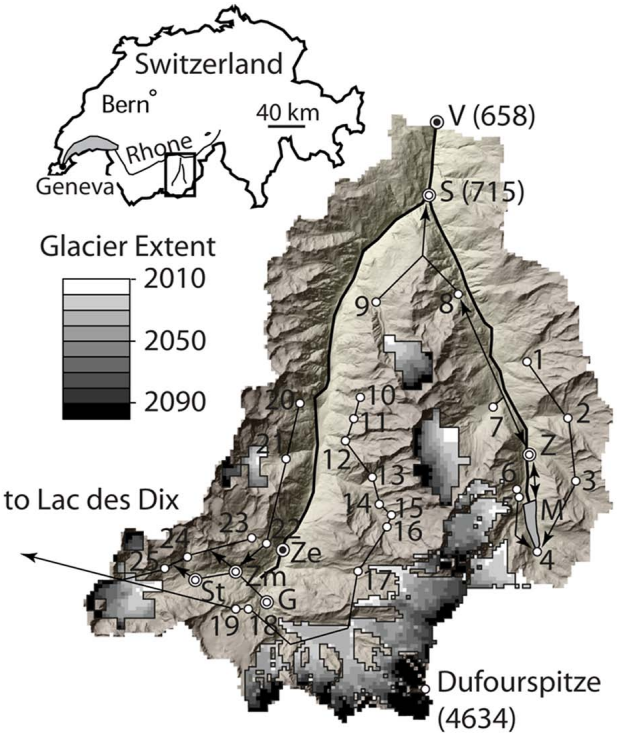

Figure 1. Vispa valley including the watershed of Mattmarksee. Dots in circles illustrate location of important landmarks, double circles are indicating hydropower facilities, and white circles locate water intakes. The color bar on the left side indicates the retreat of glacier extent in 10 year intervals. Arrows on the map illustrate water flow in pipelines of the hydropower companies. Values in parentheses indicate altitude in m asl. Details about each labeled symbol are listed in Table 4.

Switzerland. The gauging station near the village of Visp (location V in Figure 1) drains a total area of 778 km^2, which includes the Matter valley on the western part and the Saas valley on the eastern part. The average annual runoff volume of 0.53 km^{-3} a^{-1} (equivalent to 689 mm a^{-1}) measured in Visp represents about 9.3% of the total runoff from the Rhone valley as measured at the outlet into Lake Geneva. The catchment elevation ranges from 659 m asl in Visp to 4634 m asl at the Dufourspitze. About 29% of the area is covered by glaciers, containing seven larger (>5 km^2) valley glaciers. The seven major glaciers are all located at altitudes between 2287 and 4408 m asl, varying in size from 4.6 km^2 (glacier in the Schalibach watershed) to 51 km^2 (Gornergletscher, the second largest glacier system in Switzerland). Icefields, firns, and snow fields smaller than 4.6 km^2 were modeled as permanent snow fields (see section 3). Based on the simulations of *Farinotti et al.* [2011] we estimate the mean annual glacier retreat to vary between 0.05 (glacier in the Schalibach watershed) and 0.48 km^2 a^{-1} (Gornergletscher). Further topographic information on the major glaciers is summarized in Table 1 and provided in *Farinotti et al.* [2011].

[9] The natural runoff in Vispa valley is exploited by two hydropower companies, which divert parts of the runoff into two hydropower reservoirs, Mattmarksee (storage volume of 101 Mio m^3; surface: 1.76 km^2; depth: 96 m), operated by the *Kraftwerke Mattmark* (KWM), and Lac de Dix (storage volume of 400 Mio m^3; surface: 3.65 km^2; depth: 227 m) operated by *Grande Dixence* (GD). While GD has diverted water to the Lac de Dix reservoir outside the study site since 1964, Mattmarksee has been operational since 1965 and is located in the eastern valley of the catchment (location M in Figure 1). KWM operates nine water intakes, draining a total area of 162 km^2, diverting the water into Mattmarksee or down to the power plant at Stalden (location S in Figure 1). GD disposes of 19 water intakes, diverting over 400 M m^3 a^{-1} of natural runoff from a total area of 241 km^2 to Lac de Dix. Two further hydropower companies, *Energy Zermatt* and *EnAlpine* operate river power plants, which do not enact storage capacities and therefore do not affect the temporal runoff of the Vispa.

[10] While GD diverts all water collected to the Lac de Dix situated outside the Vispa valley, water storage in Mattmarksee leads to a seasonal shift of the discharge dynamics downstream of the hydropower plant. About 41% of the annual discharge in the entire Vispa valley is used for hydropower production by KWM, altering the runoff regime at the gauging station in Visp significantly. Before hydropower operations started in 1964, natural runoff in Visp reached average monthly discharge of 75 m^3 s^{-1} in summer and about 5 m^3 s^{-1} in winter, while in recent years runoff during summer reaches about 35 m^3 s^{-1} compared to 10 m^3 s^{-1} in winter (Figure 2). This is a direct effect of the hydropower operations, revealing the practice of KWM to store water during summer and release it during winter when energy prices are highest.

[11] An overview of all available observational data in the catchment is given in Table 2. The Federal Office of Meteorology and Climatology (MeteoSwiss) operates two automatic weather stations, one close to the village of Visp and one close to Zermatt (location V and Ze in Figure 1, respectively), where mean daily air temperature (T), precipitation (P), and global radiation (I) recordings are available since 1980. KWM provided 9 years of daily lake level recordings (L), natural runoff in m^3 d^{-1}collected in Mattmarksee (Q_M) and in Zermeiggern (Q_Z at location Z in Figure 1), as well as water release rates in the generating plant in Stalden (Q_S at location S in Figure 1). Snow cover extent (SC) was derived from daily satellite images recorded by the moderate resolution imaging spectroradiometer (MODIS) continuously operational since 2001 [*Hall et al.*, 2002]. In this study we used the MODIS product MOD10A1.5 (see http://nsidc.org/). Daily discharge data from the gauging station at Visp (Q_V) were provided by the Swiss Federal Office of Environment (FOEN) starting from 1903.

[12] A digital elevation model (DEM) with a 250 m spatial resolution from the *Swiss Federal Office of Topography* (Swisstopo) was used as catchment topography. The 250 m resolution appears to be a good compromise between the sparse spatial resolution of observational data and the high resolution of local topographic settings. Soil and geology properties, as well as land cover information, were obtained from digital thematic maps available from the Swiss Federal Statistical Office (FSO).

3. Methods

[13] In order to assess the impact of climate change on hydropower production, we present an integrative modeling

Table 1. Characteristics of the Individual Glacierized Subcatchments in the Vispa Valley

	2010		2050		2090		Retreat Rate		
Catchment	A[a] (km^2)	LE[b] (m asl)	A[a] (km^2)	LE[b] (m asl)	A[a] (km^2)	LE[b] (m asl)	R[c] (km^2 a^{-1})	HPC[d]	Method[e]
Mattmark	18.9	2733	6.6	3202	0.6	3343	0.23	KWM	M
Feevispa	13.9	2880	7.6	3298	2.1	3762	0.15	KWM	E
Riedbach	7.5	2399	4.1	3356	1.1	3558	0.08	KWM	E
Findelbach	18.3	2627	12.3	3115	3.1	3520	0.19	GD	M
Gornera	51.0	2287	31.6	2941	12.8	3407	0.48	GD	M
Schalibach	4.6	2382	2.5	2835	0.7	3406	0.05	GD	E
Zmuttbach	12.8	2402	6.9	2908	1.9	3444	0.14	GD	E

[a]Approximate glacierized area (A) based on 250 m grid resolution, given by the model resolution.
[b]Altitude of the lowest glacierized cell (LE) based on 250 m grid resolution, given by the model resolution.
[c]Mean annual glacier retreat (R) based on 250 m grid resolution, given by the model resolution.
[d]Hydropower company (HPC) which captures glacier runoff for hydropower production.
[e]Method used to make glacier extend projections: M: modeled by *Farinotti et al.* [2011]; E: extrapolated as described in the text.

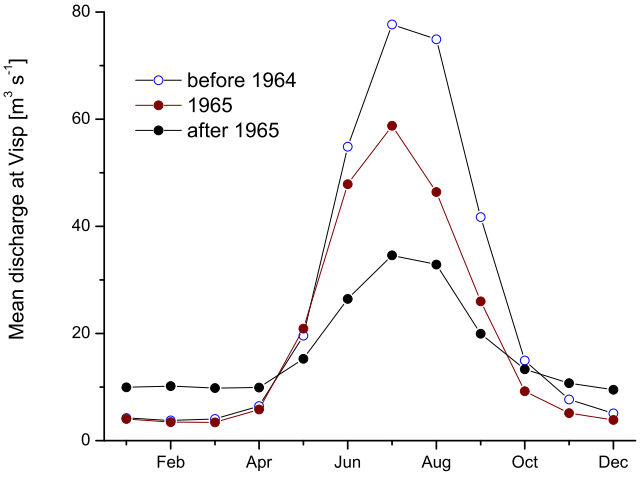

Figure 2. Monthly average discharge patterns in the Vispa River at Visp before 1964 without hydropower operations, in 1965 when water diversion to Lac de Dix started, and after 1965 when Mattmarksee was fully operational.

approach, by coupling a hydrological model with downscaled and error-corrected RCM projections, glacier retreat projections, and hydropower operational rules. In section 3 we describe the individual components of this model chain, the uncertainty they introduce into hydrological projections, and how uncertainty is analyzed in this study.

3.1. Climate Model Projections

[14] In order to drive our hydrological model we use the most comprehensive RCM ensemble available from the EU FP6 Integrated Project ENSEMBLES. ENSEMBLES is restricted to the A1B emission scenario, which is characterized by global economic growth and a balanced emphasis on all energy sources [*Nakicenovic et al.*, 2000]. However, since the emission scenarios have only a small impact on climate change until the middle of the 21st century [*Prein et al.*, 2011] this is only a minor restriction to the results of this study until 2050. For the projections until the end of the 21st century, the global mean temperature increase due to the A1B emission scenario is between the other two major scenarios used in the IPCC AR4 report [*Solomon et al.*, 2007] (B1 at the lower bound and A2 at the upper bound).

[15] *Déqué et al.* [2011, 2007] showed that the choices of the GCM as well as the RCM are major sources of uncertainty. To account for this uncertainty, we selected seven RCMs from a set of 15 available simulations that are forced by four distinct GCMs (Table 3), adequately accounting for uncertainty in boundary conditions and RCM model formulation as suggested by *van der Linden and Mitchell* [2009]. We excluded all simulations driven by the GCMs HadCM3Q3 and HadCM3Q16 because they are regarded as not realistic [*van der Linden and Mitchell*, 2009]. From the remaining RCM simulations, five simulations were forced by the global climate model ECHAM5-r3. In order to avoid an artificial bias toward the climate response of ECHAM5-r3, we limited our selection to two ECHAM5-r3 simulations. Therefore our final selection of all climate scenarios (Table 3) represents an ensemble of state of the art climate projections.

[16] In order to correct RCM errors in representative present day climate and for further downscaling [*Frei et al.*, 2003; *Hagemann et al.*, 2004; *Suklitsch et al.*, 2008; *Suklitsch et al.*, 2010], we used an innovative approach in this study, combining dynamical and statistical downscaling with observations, as proposed by *Themeßl et al.* [2011a]. This quantile based error correction approach (quantile mapping; QM) is based on the observations of the two meteorological ground stations, Visp and Zermatt, in order to produce error-corrected and downscaled RCM projections for daily mean air temperature, daily precipitation sum, and daily mean global radiation.

[17] In a first evaluation step we checked the performance of QM using the 28 years (1980–2008) of observational data from Visp and Zermatt. Mean differences (MD) and the ratio of the standard deviation (SD) between simulated and observed daily values ($R = \sigma(\text{sim})/\sigma(\text{obs})$) for all three meteorological variables are summarized in Table 3. As can be seen from Table 3, the error-corrected RCM simulations adequately reconstruct mean and variability of the local weather patterns. This is particularly true in mountainous regions, where QM proved to improve the skill of RCM simulations significantly, as discussed in detail by

Table 2. Overview of Available Data Sets

Parameter		Unit	Period	Location[a]	Resolution
	Used to Drive the Model				
T	Mean air temperature	°C	1980–2009	V, Ze	daily
P	Precipitation	mm d^{-1}	1980–2009	V, Ze	daily
I	Global radiation	W m^{-2}	1980–2009	V, Ze	daily
L	Lake level of Mattmarksee	m asl	2000–2009	M	daily
	Used to Calibrate the Model[b]				
Q_M	Total input to Mattmarksee[c] ($Q_1 + Q_2 + Q_3 + Q_5 + Q_6 + Q_Z$)	m^3 d^{-1}	2000–2009	4	daily
Q_Z	Total discharge collected at Zermeigern[d] ($Q_{Zer} + Q_7 + Q_8 + Q_9$)	m^3 d^{-1}	2000–2009	Z	daily
SC	Snow cover extent derived from satellite images	binary	2001–2009	entire catchment	daily
	Only Used to Evaluate the Model				
Q_V	Discharge in Visp	m^3 d^{-1}	1903–2009	V	daily
Q_S	Hydropower discharge release at Stalden	m^3 d^{-1}	2000–2009	S	daily

[a]Locations are marked in Figure 1.
[b]These data have been used for calibration (2004) and evaluation (2001–2008)
[c]Sum of natural discharge collected at locations 1, 2, 3, 5, 6, and total runoff collected at Z.
[d]Sum of natural discharge collected at locations Z, 7, 8, and 9.

Table 3. Performance of the Seven Selected Climate Scenarios in Representing Present-Day Climate Mean and Variability

Nr	GCM	Institute RCM[a]	MD_P (mm d^{-1})	R_P (–)	MD_T (°C)	R_T (–)	MD_I (W m^{-2})	R_I (–)
			At Zermatt[b]					
1	ARPEGE	CNRM-ALADIN5.1	−0.003	1.006	0.006	0.997	0.21	1.001
2	ARPEGE	DMI-HIRHAM5	−0.02	1.004	−0.003	0.997	0.131	0.999
3	HadCM3Q0	ETHZ-CLM	−0.02	0.984	−0.017	0.996	0.232	0.998
4	HadCM3Q0	HC-HadRM3	−0.009	1.009	−0.011	0.996	0.003	1
5	ECHAM5-r3	KNMI-RACMO2	−0.024	0.995	0.005	1	0.048	1
6	ECHAM5-r3	MPI-REMO	−0.017	0.999	0.007	1	0.032	1
7	BCM	SMHI-RCA	−0.036	0.973	0.003	0.998	0.221	0.998
			At Visp[b]					
1	ARPEGE	CNRM-ALADIN5.1	−0.01	1	−0.009	0.999	0.049	1.001
2	ARPEGE	DMI-HIRHAM5	−0.019	1.016	−0.019	0.998	0.283	0.998
3	HadCM3Q0	ETHZ-CLM	−0.025	0.992	−0.03	0.998	0.013	0.998
4	HadCM3Q0	HC-HadRM3	−0.016	1.004	−0.027	0.999	−0.128	1
5	ECHAM5-r3	KNMI-RACMO2	−0.01	0.993	−0.009	1.001	−0.077	1
6	ECHAM5-r3	MPI-REMO	−0.011	1.001	−0.014	1.001	−0.087	1
7	BCM	SMHI-RCA	−0.01	1.005	−0.008	0.998	0.203	0.998

[a]RCM scenarios for Europe are available from the ENSEMBLES project (http://ensembles-eu.org/).
[b]Values in the table indicate mean difference (MD) and the ratio of SD of simulated and observed climate variables (R) during the reference period 1980 to 2008. Index *P* stands for precipitation, *T* for air temperature, and *I* for global radiation.

Themeßl et al. [2011a, 2011b]. Furthermore, these tests confirm that the QM method can also be applied to global radiation, a finding that was not described by *Themeßl et al.* [2011a]. Nevertheless, these results do not represent the quality of QM applied to future climate simulations, since evaluation and calibrations periods are identical. A more stringent evaluation of the methods is given in *Themeßl et al.* [2011b].

[18] The variability of the projected climate change signals within the seven error-corrected RCM scenarios reveals the uncertainty of present state RCM projections for the Vispa valley. Climate change signals between the long-term period (2069 to 2098) and the representative reference period of the current climate (1992 to 2019; see section 3.3.4) vary between +3.2 and +4.7°C warming during the melt season (May to September) and +1.6 and +3.0°C during the low flow season (January to April; see Figure 3). Since the RCMs have a grid spacing of about 25 km and an effective resolution of at least four times this value, spatial differences in the projections for the two weather stations, which are only about 35 km apart, can only be achieved by applying empirical-statistical methods like QM, which introduce local climate information from the stations. For example, the weather station at Visp records typical weather patterns for the lower valley (e.g., stratus formations), and at Zermatt typical weather patterns for the upper valley are recorded (e.g., adiabatic winds) [*Rüedlinger*, 2010]. On average, the seven scenarios project slightly higher temperature increase during the melt season in Zermatt (mean increase: +4.3°C) than in Visp (mean increase: +3.7°C). During the low flow season, the multimodel average warming is quite similar with +2.2°C in Zermatt and +2.3°C in Visp. Fairly similar signals can be observed for precipitation. In Zermatt, precipitation is projected to increase by an average of +11.5% during low flow season but decrease during the melting season by −13.4%. In Visp, an increase of precipitation during low flow of +14.8% and a decrease during melt season of −3.5% is projected. On average, the selected scenarios project a decrease in mean global radiation of up to 4.2 W m^{-2}. Nevertheless, some scenarios also predict an increase of mean radiation of up to +9.3 W m^{-2} (Figure 3).

3.2. Glacier Model Projections

[19] The hydrological model used in this study can only account for glacier ice melt and snow accumulation, disregarding glacial dynamics and retreat. We therefore rely on externally determined evolution of glacier masks for model projections up to the year 2100. The ice volume changes of the biggest glaciers in the Vispa catchment have been monitored throughout the last century [*Bauder et al.*, 2007]. *Farinotti et al.* [2011] used a glacier evolution model [*Huss et al.*, 2008] that includes all important processes of accumulation and melt of snow and ice as well as the dynamic response of the ice masses to evaluate the transient evolution of the ice volume, glacier covered area, and the distributed mass balance until 2100 of the three highly glacierized subcatchments, Gornera, Findelbach, and Mattmark (Table 1). The future projections are based on ten regional climate change scenarios derived from the ENSEMBLES project [*van der Linden and Mitchell*, 2009] as described by *Bosshard et al.* [2011]. Although the climate scenarios used to drive the glacier model in the study of *Farinotti et al.* [2011] slightly differ from those used to drive the hydrological model in this study, they can be considered as largely consistent since mostly the same climate simulations are used, all driven by the A1B emission scenario.

[20] Projections of the remaining smaller glaciers in the catchment, for which detailed simulations were not available due to lack of observational data, we used an elevation dependent linear retreat as projected for the three simulated glaciers. We justify this simplification for the smaller glaciers by the fact that the three biggest glaciers, for which explicit modeling is available, account for over 69% of the glacierized area (Table 1). The results of *Farinotti et al.* [2011] demonstrate that the glacier retreat is a continuous gradual process, rendering our approach to use externally determined glacier extents with a 250 m spatial resolution,

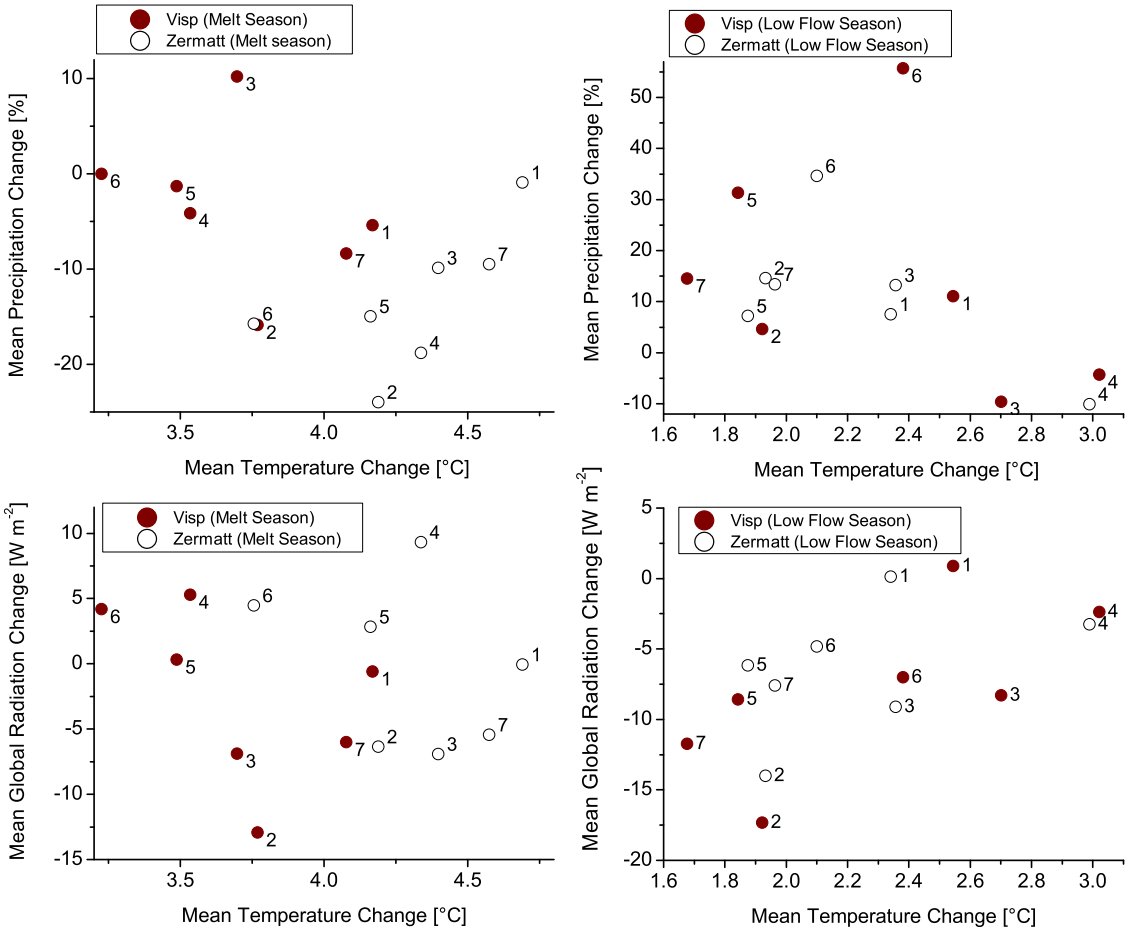

Figure 3. Climate change signals in mean air temperature, precipitation, and global radiation between the reference period (1992–2019) and the end of the century (2071–2098) during low flow (January to April) and melt season (May to September). Labels indicate specific climate scenarios as listed in Table 3.

valid. The evolution of the projected glacier extents are illustrated in Figure 1 and summarized in Table 1.

3.3. Hydrological Modeling and Projections

3.3.1. Model Setup

[21] The modified *topographic kinematic approximation and integration* model (TOPKAPI) is a physically based rainfall-runoff model [*Todini and Ciarapica*, 2001], developed from the conceptual ARNO model [*Todini*, 1996]. In this study we used a modified version of TOPKAPI almost identical to the version used by *Finger et al.* [2011]. The modified version contains the enhanced temperature index (ETI) model, which computes ice and snow melt rates based on ambient temperature and solar radiation using a constant temperature factor (TF) and short wave radiation factor (SRF) [*Pellicciotti et al.*, 2005]. The water routing in TOPKAPI is based on the kinematic wave concept, which can lead to numeric problems when fluctuation is very large. While in this study this was never the case for simulation of the present climate, about 1.6% of simulated future time periods revealed numeric problems and were hence not considered in the results.

[22] For the model setup of the Vispa valley study site, the DEM with 250 m grid resolution provided by Swisstopo was used. According to the digital soil and land use maps from the FSO, 97% of the watershed can be characterized as glaciers, ridges, steep slopes, or high alpine, with the according soil characteristics (Table 5). Similarly, four land use types were defined, assigning each one according Manning's coefficients and crop factors (Table 5). The channel geometry in the entire catchment is assumed to be rectangular with decreasing width according to the distance from the outlet of the catchment. For calibration purposes the glacier extent of 2010 was used, which seems appropriate as glacier retreat within one decade is below the spatial grid resolution of our model (Figure 1).

[23] The model is driven with daily meteorological data (P and T) recorded at the MeteoSwiss station at Visp, located at 640 m asl, and at Zermatt at 1626 m asl (Figure 1). Data from the meteorological station of Zermatt was used to extrapolate P and T above 1600 m asl and data from Visp was used to extrapolate P and T below 1600 m asl. Radiation is computed by the hydrological model, accounting for daily cloud cover according to the parameterization proposed by *Pellicciotti* [2004], which relies on daily

maximum and minimum air temperatures available at Zermatt and Visp.

3.3.2. Modeling Hydropower Operations With TOPKAPI

[24] The main modification to the TOPKAPI version used by *Finger et al.* [2011] is the implementation of a reservoir module [*Todini and Mazzetti*, 2008], to account for storage in reservoirs, water abstraction, diversion of natural mountain streams and routing of pressurized water to turbines. The discharge released from the reservoir is determined by the means of user provided lake level time series, as originally described by *Todini and Mazzetti* [2008]:

$$Q_{\mathrm{res}}(t) = Q_{\mathrm{M}}(t) + P_{\mathrm{res}}(t) \cdot A_{\mathrm{res}} - \Delta V_{\mathrm{res}}(h) \quad (\mathrm{m^3 d^{-1}}), \quad (1)$$

where Q_{res} denotes the discharge from the reservoir, Q_{M} stands for total natural runoff and diverted water input to the reservoirs, P_{res} stands for the precipitation above the reservoir area A_{res}, and $\Delta V_{\mathrm{res}}(h)$ represents the observed volume change depending on the lake level observations and the bathymetric map, between the present and the previous time step. If $\Delta V_{\mathrm{res}}(h)$ becomes greater than the input into the reservoir the discharge from the reservoir is stopped by setting Q_{res} to 0. This constraint prevents Q_{res} from becoming negative and allows the model to compensate short-term underestimations of simulated inflow to the reservoir as discharge from the reservoir is stopped until the simulated lake level reaches the observed lake level again.

[25] Water extraction, diversion of mountain streams, and routing of pressurized water to the turbines were implemented by subtracting the amount of water diverted from the river cell flowing through a water frame and adding it to the target river cell. The hydropower operational rules in the Vispa valley can be limited within our study to the activities of GD and KWM, as other hydropower activities (e.g., *Energy Zermatt* and *EnAlpin*) are irrelevant for our study since they do not affect natural runoff beyond a daily time scale. All the operational rules for the specific case of GD and the KWM are summarized in Table 4 and visualized in Figure 1. KWM collects water at five intakes (locations 1, 2, 3, 5, and 6) and diverts it to the Mattmarksee (M). Water collected at locations 7, 8, 9, and in Zermeiggern (Z) is stored in our model in one single reservoir, the Mattmarksee. This is a simplification, as in reality water can be released directly to Stalden (S), or be pumped up

Table 4. Overview of Water Intakes of KWM and GD

Loc.[a]	Name	X (m)[b]	Y (m)[b]	H (m asl)	$Q_{\max}$ ($\mathrm{m^3\ s^{-1}}$)	Diversion
			Saas Valley			
1	Trift	640,467	109,477	2291	5.5	diverted to 4
2	Almageller/Rottal	642,911	105,545	2280	4.6	diverted to 4
3	Furg	643,225	101,306	2282	3.8	diverted to 4
4	Inflow Mattmarksee	–	–	2197	–	inflow to lake
5	Hohlaub	639,624	100,796	2219	3.5	diverted to 4
6	Allalin	639,729	100,292	2255	3.5	diverted to 4
7[c]	Saas-Fee	637,747	106,569	1770	14.0	diverted to 4
8[c]	Schweiben	635,482	113,739	1772	1.5	diverted to 4
9	Riedbach	630,376	113,087	1823	3.0	diverted to 4
Z[c]	Zermeiggern	640,055	102,997	1770	3.0	diverted to 4
S	Stalden	–	–	715	–	outlet to river
M[d]	Mattmarksee	–	–	2197	–	released to S
V	Visp	634,150	124,850	658	–	gauging station
			Matter Valley			
10	Hohberg	629,295	106,863	2534	2.4	diverted to LdD
11	Festi	628,833	105,351	2548	2.3	diverted to LdD
12	Kin	629,393	103,730	2764	1.9	diverted to LdD
13	Rotbach	629,866	101,453	2548	1.5	diverted to LdD
14	Alphubel	630,535	99,525	2571	1.3	diverted to LdD
15	Mellichen	631,150	98,372	2637	6.0	diverted to LdD
16	Längflue	630,822	97,817	2598	1.3	diverted to LdD
17	Findelbach	629,087	94,919	2508	17.7	diverted to LdD
18	Obertheodul	621,631	92,814	2486	4.5	diverted to LdD
19	Furgg	620,781	92,823	2487	6.6	diverted to LdD
20	Bis	624,851	106,159	2168	3.4	diverted to Zm
21	Schalibach	624,004	102,869	2128	10.0	diverted to Zm
22	Edelweiss	–	–	~2078	5.0	diverted to Zm
23	Trift	621,469	98,095	2442	7.0	diverted to LdD
24	Arben	617,554	96,190	2554	2.3	diverted to LdD
25	Hohwäng	616,065	95,388	2612	2.0	diverted to LdD
G[e]	Gornera	622,600	93,211	2007	12.0	diverted to LdD
St	Stafel	618,125	94,900	2212	10.0	diverted to LdD
Zm[e]	Z'mutt	620,990	95,179	1970	7.0	diverted to LdD residual to G

[a]Locations are illustrated in Figure 1.

[b]Swiss coordinate system using the geodetic datum CH1903.

[c]Mathematical simplification 1: water collected at these locations is diverted to 4, as M in the model acts as reservoir including all water stored in the entire system.

[d]Mathematical simplification 2: water from M is directly released to S, as M accounts for all water stored in the system.

[e]Mathematical simplification 3: at Z'mutt 7 $\mathrm{m^3\ s^{-1}}$ are directly pumped to Lac de Dix (LdD) the rest is diverted to G. At G 12 $\mathrm{m^3\ s^{-1}}$ is diverted to GD the rest is released as residual flow.

from Z to M. As storage volume in the pipes and at Zermeiggern is negligible, mathematically it does not matter if water is stored in the pipes, at Z or in M. Therefore we simplify the hydropower installations with one single reservoir, the Mattmarksee. The water released from this reservoir is defined by lake level observations (equation (1)). KWM also operates historic turbines in Saas Fee, but these are being neglected in our modeling approach, as they are rarely used and do not affect runoff beyond a daily basis.

[26] GD collects water at 13 water intakes (at location 10, 11, 12, 13, 14, 15, 16, 17, 18, 19, 23, 24, and 25) and diverts it directly to the Lac de Dix outside the catchment. At Stafel, water is collected and diverted (through pumps) to GD. The pumps can only reach a capacity of 10 $m^3\ s^{-1}$. The rest is released downstream, but collected at Z'mutt (location Zm). Water collected at 20, 21, and 22 is diverted to the cell upstream of Z'mutt. At Z'mutt water coming from 20, 21, 22, and from the upstream basin is pumped to GD with a Q_{max} of 7 $m^3\ s^{-1}$. The remaining water is diverted to Gornera (G). This is again a simplification, as in reality no water is diverted from Zm to G. At Gornera (G) water is being diverted to GD with a Q_{max} of 12 $m^3\ s^{-1}$. This is also a simplification, as in reality water is being diverted to Zm. However, at Zm there are two pumps which have a Q_{max} of 12 $m^3\ s^{-1}$. Consequently, first water from the upstream basin is pumped to GD, before water from G is pumped. Accordingly, we simplify this by first diverting all surplus water (>7 $m^3\ s^{-1}$) from 20, 21, and 22 to G and limiting the diversion of water at G to GD to 12 $m^3\ s^{-1}$.

3.3.3. Stochastic Model Calibration

[27] We use a stochastic model calibration technique proposed by *Finger et al.* [2011] which identifies physically plausible parameter sets, resulting in good model performance regarding all available observational datasets. Using this technique, *Finger et al.* [2011] demonstrated that the combination of satellite snow cover images and discharge data leads to a high internal consistency, making it suitable for climate change predictions. In the present study we extended the technique to also assess the uncertainty of model projections. The technique has been presented in detail by *Finger at al.* [2011], therefore here we only outline the specific adaptations and extensions necessary for the present study.

[28] We first generated 10,000 random parameter sets from a uniform and physically plausible constrained range indicated in Tables 5 and 6. Although 10,000 parameter sets cannot sample the entire parameter space, many authors have demonstrated that this number is sufficient to obtain adequate model efficiency [*Beven and Binley*, 1992; *Finger et al.*, 2011; *Seibert and Beven*, 2009; *Uhlenbrook and Sieber*, 2005]. Furthermore, as only the headwaters are diverted into Mattmarksee, the relevant areas of the Vispa valley are comparable to the Rhonegletscher study site investigated by *Finger et al.* [2011], making their approach also suitable for the Vispa valley. In accordance with *Finger et al.* [2011], the saturated hydraulic conductivity parameter K_{sh} was generated from a log-uniform distribution. The initial range of K_{sh} was defined to vary over several magnitudes to allow the model to mimic runoff through coarse gravel as well as through glacier pulp (Table 5). Although TOPKAPI disposes of the option for a second soil layer, we refrained from using this option to avoid overparameterization of the model. All initial parameter ranges were defined based on experience and experimental data as described by *Finger et al.* [2011].

[29] Efficiency criteria were used to quantify the model performance regarding total natural and diverted runoff into Mattmarksee (Q_M), total discharge from the lower intakes collected at Zermeiggern (Q_Z), and correctly predicted snow cover area (SC). Performances of all simulated discharges were surveyed using the Nash-Sutcliffe coefficient (E_Q) [*Nash and Sutcliffe*, 1970]:

$$E_{Q,j} = 1 - \frac{\sum_{i=1}^{n} (Q_{i,j,\mathrm{obs}} - Q_{i,j,\mathrm{sim}})^2}{\sum_{i=1}^{n} (Q_{i,j,\mathrm{obs}} - \overline{Q_{i,j,\mathrm{obs}}})^2}, \quad (2)$$

where index i represents the time steps, index j stands for the respective location, Q_{obs} stands for observed discharge, and Q_{sim} depicts simulated discharge. Furthermore, the

Table 5. Summary of the Soil Parameters

Soil Parameters		Unit	Glacier	Ridges	Steep Slopes	High Alpine
Soil depth, d_1	ir[a] m; σ[a]	m	0.25–1.5 0.74; 0.31	1–6 2.9; 1.25	0.75–4.5 2.22; 0.93	1.5–9 4.4; 1.87
Horizontal saturated hydraulic conductivity,[b] K_{sh}	ir m; σ	m h^{-1}	$1e^{-12}$–$1e^{-8}$ $5e^{-9}$; $3e^{-9}$	$1e^{-5}$–$1e^{-1}$ $5e^{-2}$; $4e^{-2}$	$1e^{-5}$–$1e^{-1}$ $5e^{-1}$; $4e^{-1}$	$1e^{-5}$–$1e^{-1}$ $5e^{-2}$; $4e^{-2}$
Vertical saturated hydraulic conductivity,[c] K_{sv}		m h^{-1}	0.2* K_{sh1}	0.2* K_{sh1}	0.2* K_{sh1}	0.2* K_{sh1}
Saturated soil moisture content, θ_s	ir m; σ	–	0.2–0.6 0.35; 0.13	0.1–0.3 0.18; 0.07	0.15–0.45 0.27; 0.1	0.1–0.3 0.18; 0.07
Residual soil moisture content,[d] θ_r	const.	–	0.2	0.2	0.2	0.2

Surface and Vegetation Parameters	Unit	Alp. Pastures	Unprod. Veg.	Surf. Without Veg.	Slightly Dev. Lands
Manning's coeff.	–	0.35	0.03	0.025	0.03
Crop factor	–	0.4–1	0.4–1	0.4–1	0.4–1

[a] ir stands for initial range; m stands for mean of 10 best parameter sets, and σ stands for SD of the respective mean.
[b] K_{sh} values were generated from a log-uniform distribution for Monte Carlo runs.
[c] In order to minimize the number of parameters to be varied θ_{r1} was kept constant and K_{sv} was made dependent on K_{sh}.
[d] θ_r was kept constant to minimize varying model parameters.

Table 6. Summary of the Melt Parameters Required By the Melt Model Component of TOPKAPI

Parameter		Unit	Value Range	m[a]	σ[b]
T_t	threshold air temperature for melt	°C	−2 to +2	−0.926	0.474
$T_{t,P}$	threshold air temperature for precipitation state transition (solid/fluid)	°C	−2 to +2	−0.926	0.474
T_{onset}	threshold temperature for N_{day}[c]	°C	−2 to +2	−0.926	0.474
T_{grad}	temperature gradient with elevation	°C m^{-1}	0.002–0.007	0.006	0.0006
T_{mod}	temperature decrease over glacier area	°C	0–2	1.231	0.7059
SRF	shortwave radiation factor	m we m^2 W^{-1} h^{-1}	0–14	0.0122	0.0012
TF	temperature factor	m we C^{-1} h^{-1}	0–400	0.1046	0.0463
p_1	first albedo factor	–	0.7–1	0.9377	0.0510
p_2	second albedo factor	–	0.1–0.2	0.1334	0.0272
α_G	glacier ice albedo	–	0–0.4	0.1221	0.1109
α_{ground}	average basin wide ground albedo	–	0.2–0.3	0.2512	0.0358
K_{snow}	storage constant for snow melt and rain on glaciers	h	5–100	51.97	26.35
K_{ice}	storage constant for ice melt and channel inflow of glaciers	h	5–100	51.35	21.76
P^{su}_{prec}	precipitation gradient with elevation from May to Oct	m^{-1}	0.01–0.06	0.0484	0.0072
P^{wi}_{prec}	precipitation gradient with elevation from Nov to Apr	m^{-1}	0.055–0.33	0.2663	0.0395

[a] m stands for the mean of the 10 best parameter sets.
[b] σ stands for the SD of the mean of the 10 best parameter sets.
[c] T_t, $T_{t,P}$, and T_{onset} were set equal to minimize numbers of parameters to be varied. N_{day} was kept constant at 1 day.

accumulated volume error of total input into Mattmarksee (E_{VE}) was computed for each run as follows:

$$E_{\text{VE}} = \sum_{i=1}^{n} |Q_{i,j,\text{obs}} - Q_{i,j,\text{sim}}|. \quad (3)$$

[30] Predicted snow cover was evaluated by determining the daily ratio of correctly predicted snow cover area (E_{CPSC}) as follows:

$$E_{\text{CPSC}} = \frac{c_{\text{corr}}}{c_{\text{tot}} - c_{\text{missing}}}, \quad (4)$$

where c_{corr} stands for the number of correctly predicted cells, c_{tot} stands for the total of cells in the catchment, and c_{missing} accounts for the number of cells with no data due to cloud cover.

[31] Based on these efficiency criteria, the 10,000 Monte Carlo runs were ranked regarding the performance of the four above mentioned efficiency criteria. For this purpose we defined a ranking value P^i_r for each run r and each efficiency criterion k as

$$P^k_r = \frac{(N+1) - \text{Rank}^k_r}{N}, \quad (5)$$

where N is the total number of runs performed and R stands for the rank of the considered run with regard to the efficiency criterion k. Thus, ranking values were defined for each data set used for calibration, namely $P^{E_Q}_r$ and $P^{E_{\text{VE}}}_r$ of Q_M, $P^{E_{\text{CPSC}}}_r$ in the entire catchment and $P^{E_Q}_r$ of Q_Z. Aggregated ranking values for the best run with respect to $E_{Q,M}$ and $E_{Q,Z}$, lowest E_{VE} and best E_{CPSC}, were determined by averaging the corresponding ranking values according to equation (6):

$$P^{OA}_r = \frac{1}{4}(P^{E_{Q,M}}_r + P^{E_{Q,Z}}_r + P^{E_{\text{VE}}}_r + P^{E_{\text{CPSC}}}_r). \quad (6)$$

[32] The runs with the highest P^{OA}_r were defined as the runs with the best overall performance

[33] To keep computational time at a reasonable level we limited the calibration period to one representative average year (1 January 2004 to 31 December 2004), only in order to challenge the model by surveying its performance during an 8 year evaluation period (2001–2008), including the extreme heat wave of the year 2003 [*Schär et al.*, 2004]. In order to initialize the water content in soil and streams, as well as the seasonal snowpack, we included in each calibration run a 12 month spin up period.

3.3.4. Climate and Glacier Forced Hydrological Projections and Their Uncertainty

[34] Future hydrological projections are subject to uncertainty due to (i) natural climate variability, (ii) uncertainty in anthropogenic climate forcing by the emission of greenhouse gases, (iii) uncertainty in the formulation of climate models, (iv) parameter uncertainty (calibration and setup) in hydrological models, and (v) uncertainty in the future projection of glacier extent.

[35] As argued in section 3.1, emission scenario uncertainty is not a focus of our study, as only the A1B emission scenario is used [*Nakicenovic et al.*, 2000]. Uncertainties in the formulation of global and regional climate models are regarded by applying seven different GCM-RCM combinations (Table 3). Uncertainties due to internal variability of the GCMs and RCMs are not regarded separately, but are to some degree implicitly included in the different GCM-RCM combinations. The seven climate scenarios adequately represent the uncertainty of state of the art RCM projections, as discussed in section 3.1. Natural climate variability is intrinsically sampled by assessing the interannual variability within the projected 28 year time periods (section 3.4.2). As TOPKAPI computes distributed global radiation internally, with a user defined daily cloud factor, we projected cloud factors for future time periods based on the projected daily mean global radiation divided by the 28 year maximum of the specific month global radiation up to the end of the 21st century.

[36] Concerning the uncertainty in future projection of glacier extent, the glacial retreat is predicted by simulations presented by *Farinotti et al.* [2011]. The average horizontal retreat in most areas is less than 25 m per year, making it only possible to account for glacier retreat in decadal intervals, as the spatial resolution of our model is 250 m. Accordingly, in order to account for uncertainty in future projections, we force the hydrological model for the medium-term time period with the extents projected by

Farinotti et al. [2011] of the years 2040, 2050, and 2060 and for the long-term time period with the extents of 2070, 2080 and 2090 (Figure 1). As standard deviations of the ten projected glacier extents for a particular decade are smaller than the 28 year change of glacierized area [*Farinotti et al.*, 2011], it can be assumed that the three glacier extents for each time period adequately account for uncertainty in the glacier extent projections.

[37] Parameter uncertainty in the hydrological model is sampled by using the 10 best model parameter sets, defined by the highest P_r^{OA} (equation (6)). *Finger et al.* [2011] demonstrated that reducing the number of considered best parameter sets to 10 increases the uncertainty of parameter estimation. By using only the 10 best parameter sets, we are assessing a higher uncertainty as if we considered more parameter sets, making the uncertainty due to parameter estimation rather large. Uncertainty due to the specific structure of TOPKAPI could not be assessed, as this would require the application of hydrological models with different structures, which is not the objective of the present study.

[38] The 7 climate scenarios, 10 plausible hydrological model parameter sets, and 3 glacier extents were used to perform hydrological projections for (i) a current reference time period which covers the decade before and after the evaluation period, namely from 1992 to 2019, (ii) a medium-term future time period, from 2037 to 2064, and (iii) a long-term future time period from 2071 to 2098. Altogether we performed for each of the two future time periods 210 projections, which allow us to perform a comprehensive uncertainty analysis as discussed in section 3.4.2. Similarly to the calibration procedure, all runs were started 2 years earlier to obtain an adequate spin up period.

3.4. Uncertainty Analysis of the Model Chain

3.4.1. Uncertainty of Mean Discharge

[39] The uncertainty analysis focuses on the change of future total inflow into Mattmarksee compared to present total inflow ($\Delta Q_M = Q_{M,\text{future time period}} - Q_{M,\text{present time period}}$) since it is the most important result of our study with regard to future hydropower production. The global uncertainty of ΔQ_M was assessed by first computing climatological monthly averages for the two projected future time periods (medium term and long term) of Q_M for all 210 projected simulations, defined thereafter as the multisimulation mean. Likewise, multisimulation climatological monthly averages for the reference time period of Q_M were computed, using the observed glacier extent from 2010. Subsequently, monthly ΔQ_M for each of the future time period and simulation is computed by subtracting the climatological monthly mean Q_M of the current reference period from the 28-year monthly average Q_M of the respective future time period. Hence, global uncertainty for each month in future time period is given by the variance of the 28 year multisimulation average ΔQ_M.

[40] In order to partition the global uncertainty into the uncertainty generating components, we performed an analysis of variance (ANOVA) of ΔQ_M for the two future time periods, as described by *Storch and Zwiers* [2003]. The three-way ANOVA analysis was performed regarding the three components of uncertainty, namely (i) the 7 climate scenarios, (ii) the 10 model parameter sets, and (iii) the 3 glacier extents. Based on the 210 projected monthly changes for each of the two future periods and the three uncertainty components, monthly sum of squares for each component were determined. Furthermore, monthly sums of squares concerning the nonlinear interaction between factors and the residual error are computed. In order to determine the contribution of each specific component, interaction term, and residual error to the global uncertainty, the corresponding ratios between component specific sum of squares and total sum of squares are calculated. This allows us to allocate the monthly uncertainty propagated to the end result by each uncertainty generating component, the interaction of components, and the residual error.

3.4.2. Uncertainty of Discharge Due to Natural Climate Variability

[41] Natural runoff in Alpine regions is characterized by high interannual variability, as each year is characterized by different climatic patterns [*Bartolini et al.*, 2009; *Lambrecht and Mayer*, 2009]. Furthermore, some state of the art RCMs indicate increasing interannual variability for the Alpine region with ongoing climate change [*Heinrich and Gobiet*, 2011]. In order to demonstrate how long-term changes in the mean compare to the interannual variability we compare the climatological mean of the two future periods with their interannual variability. Similar to the uncertainty analysis described in section 3.4.1, we first computed the climatological monthly mean values of the reference period for each simulation. Subsequently, interannual variation of the monthly ΔQ_M was determined by subtracting the climatological monthly mean values of the reference period from the 28 monthly multisimulation (all 210 simulations) mean Q_M of the respective future period for each simulation year. Interannual variability is then defined as the square root of the 28 multisimulation averaged variance of the ΔQ_M values.

4. Results

4.1. Evaluation of Hydrological Model Performance

[42] The performance of the hydrological model is assessed during an 8 year period from 2001 to 2008, including the calibration year 2004. The ensemble of the best 10 simulations (out of the 10,000) with the highest P_r^{OA} (equation (6)) corresponds to those runs which reveal best performance regarding E_Q of total water inflow to Mattmarksee (Q_M) and water collected at Zermeiggern (Q_Z), lowest E_{VE} of Q_M and best daily snow cover extent in the entire catchment. In Figures 4 and 5 the model performance regarding lake level of Mattmarksee (L), natural and diverted inflow to Mattmarksee (Q_M), natural discharge collected at location Z (Q_Z), total water released from the reservoir (Q_S), accumulative water released from reservoir (Q_{Sacc}), discharge observed at Visp (Q_V) and correctly predicted snow cover ratio (CPSC) are illustrated for the calibration period and the evaluation period, respectively. Numerical values of the efficiency criteria are summarized in Table 7, distinguishing between calibration period and validation period.

[43] As the model is driven by observations of L, simulated L almost perfectly matches observed L. Accordingly,

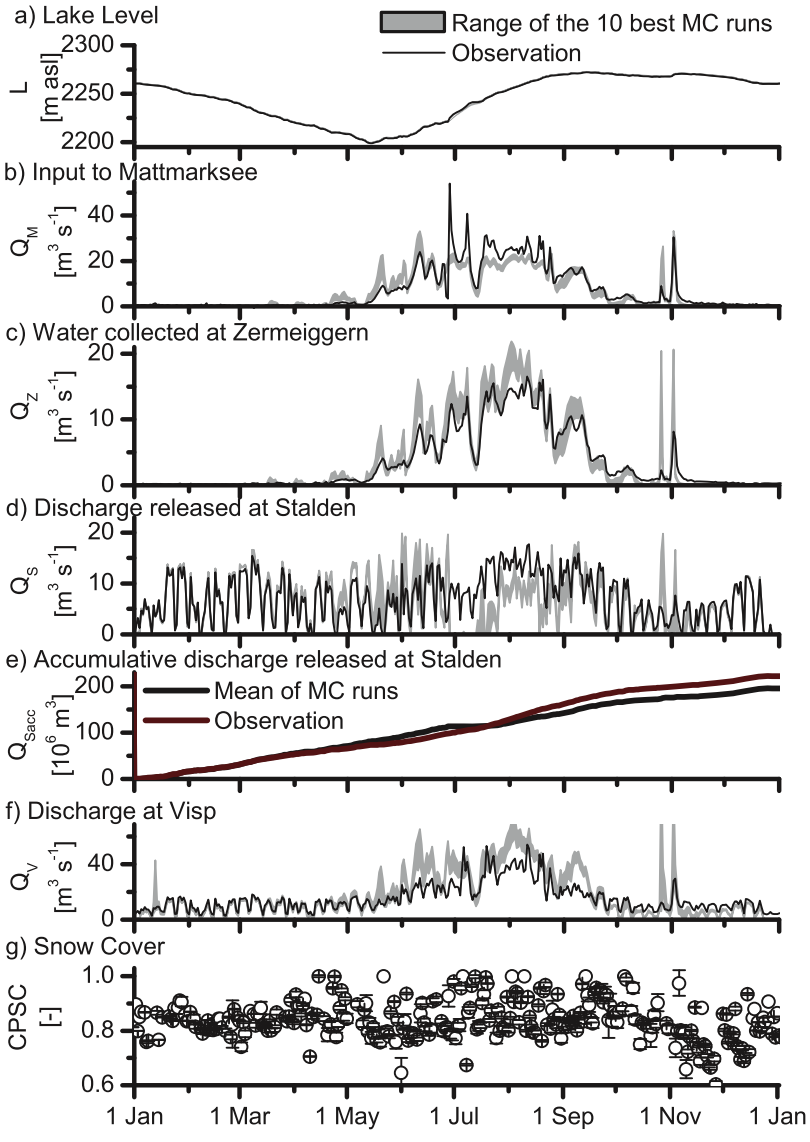

Figure 4. Model performance of the 10 best MC simulations with the best overall performance P_r^{OA} during the calibration year 2004. (a) Illustrates lake level of Mattmarksee, (b) shows total water amount available for hydropower, (c) depicts runoff collected at location Z, (d) depicts water released at Stalden, (e) demonstrates the accumulative error of simulated water release in Stalden, (f) pictures discharge in Visp, and (g) illustrates the ratio of correctly simulated snow cover in the entire catchment. Grey area indicates the range of the 10 best MC runs. Error bars in (g) show the standard deviation from the mean correctly predicted snow cover if it is greater than 0.

the Nash values for L are close to 1 (Table 7). More importantly, the total inflow to Mattmarksee is also very well predicted by the model. During the calibration year 2004 and during the entire evaluation period, mean Nash values of 0.81 and 0.78 are obtained, respectively. As illustrated in Figures 4 and 5b, efficiency is particularly reduced during and after heavy precipitation events. We discuss possible reasons for this discrepancy in section 5. However, the seasonal dynamics are predicted very well. Total water collected at the pumping station Zermeiggern (Q_Z) is also predicted reasonably well, revealing mean Nash values of 0.83 during calibration and 0.72 during the entire evaluation period. In particular, Q_Z is overestimated during heavy precipitation events as well as during strong melting periods in summer. As a consequence of the good agreement of simulated total water input into Mattmarksee, discharge released by the hydropower company at Stalden (Q_S) is also simulated adequately (Figures 4d and 5d). Deviations of simulated Q_S from observed Q_S are a direct consequence of discrepancies in the input to Mattmarksee. Accordingly, Q_S is slightly overestimated in May and June, but underestimated in August and September. Although the accumulative errors of Q_S may become important for short time periods (Figure 4e), they are averaged out over the course of several years (Figure 5e). While the mean volume error of predicted Q_S during the calibration year 2004 is 12% of the observed Q_S, it is significantly less over the entire 8 year evaluation period, accounting for about 3% of

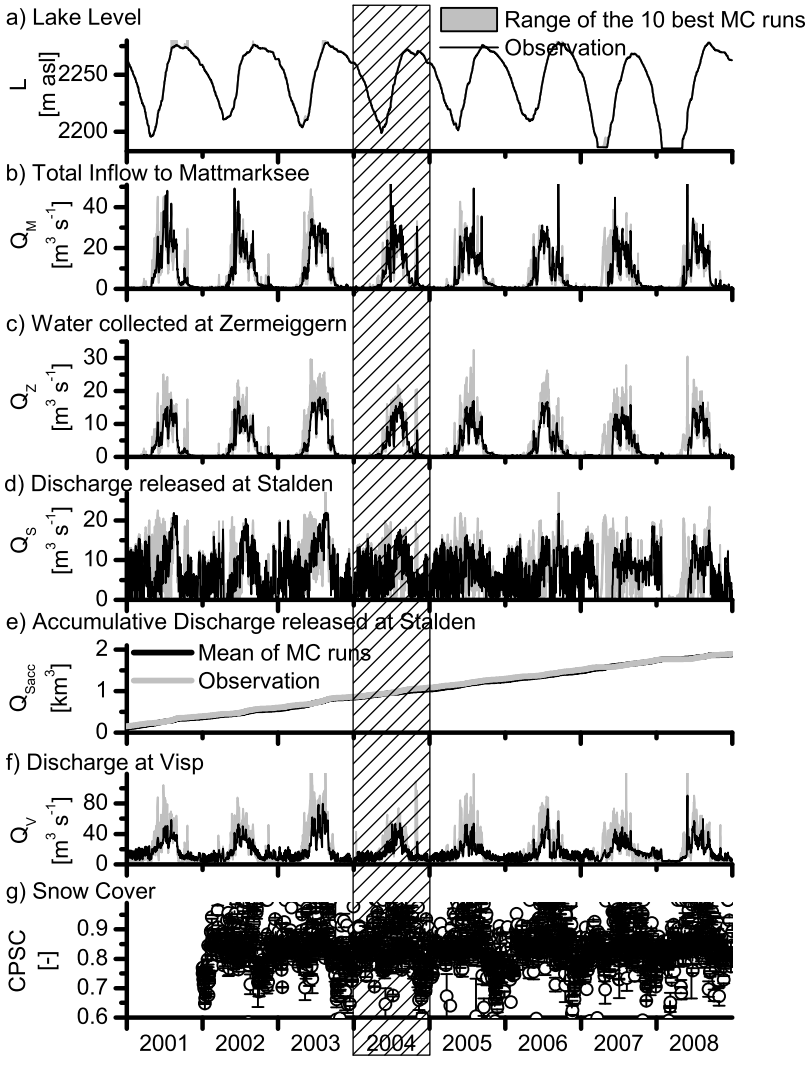

Figure 5. Model performance of the 10 best MC simulations with the best overall performance P_r^{OA} during the entire evaluation period (2001–2008; striped area marks the calibration period). (a) Illustrates lake level of Mattmarksee, (b) shows total water amount available for hydropower, (c) depicts runoff collected at location Z, (d) depicts water released at Stalden, (e) demonstrates the accumulative error of simulated water release in Stalden, (f) pictures discharge in Visp, and (g) illustrates the ratio of correctly simulated snow cover in the entire catchment. Grey area indicates the range of the 10 best MC runs. Error bars in (g) show the standard deviation from the mean if it is greater than 0.

observed Q_S (Table 7). Hence, short term errors in Q_S are averaged out by the model over longer time periods, revealing the robustness of the model calibration. Efficiency of discharge at Visp (Q_V) shows similar model efficiency as observed for Q_S. Errors revealed in Q_S during the summer time are propagated down to the gauging station in Visp, leading to an overestimation during May and June and an underestimation in July and August. Generally, Q_V is underestimated by the model, indicating inadequate model parameters for the western side valley, which was, however, not subject to model calibration.

[44] Finally, snow cover extent is predicted with a mean efficiency of over 0.83 throughout the calibration and evaluation period. The good performance of snow cover and natural discharge during the entire evaluation period confirms that the calibration is adequate for both wet and dry years. This supports the suitability of the model for climate change projections, as also discussed by *Finger et al.* [2011]. The mean values of the 10 best parameter sets (Tables 5 and 6) turn out to be similar to those values obtained by *Finger et al.* [2011], indicating that the determined values are physically plausible. In particular, the values of SRF and TF are different from the values found by *Finger et al.* [2011], but are very similar to the values determined deterministically by *Carenzo et al.* [2009] for the adjacent study site Haut Glacier d'Arolla.

4.2. Climate Change Impact on Hydrology

[45] In Figure 7 climatological monthly mean values of relevant projected variables are illustrated for the three time periods: (i) reference period from 1992 to 2019; (ii) medium-term projection from 2037 to 2064, and (iii) long-term projection from 2071 to 2098.

Table 7. Efficiency of the Ensemble of Plausible Hydrological Simulations

			Calibration Year (2004)			Evaluation Period (2000–2008) (Excluding Calibration Year 2004)		
Criterion	Variable	Location	Mean	Max	Min	Mean	Max	Min
			Used for Calibration					
$E_{Q,M}$ (–)	Q_M	4	0.81	0.87	0.81	0.78	0.86	0.71
$E_{Q,Z}$ (–)	Q_Z	Z	0.83	0.93	0.69	0.72	0.84	0.45
E_{CPSC} (–)	SC	Entire site	0.84	0.84	0.84	0.83	0.83	0.82
E_L (–)	L[a]	M	1	1	1	1	1	1
E_{VE} (10^6 m^3 a^{-1})	Q_M	4	26			3		
			Only used for evaluation					
E_{VE} (10^6 m^3 a^{-1})	Q_S[b]	S	26.8	45.5	12.0	7	20.5	−25.8
RVE[c] (–)	Q_S	S	0.12	0.21	0.05	0.032	0.09	−0.12
E_{VE} (10^6 m^3 a^{-1})	Q_V[d]	V	−73.5	29.4	−138	−100	56.2	−170.4
RVE[c] (–)	Q_V	V	−0.14	0.06	−0.26	−0.19	0.11	−0.32

[a] L was used to drive the model (equation (1)), accordingly it was not used for calibration and gives a perfect fit as long as there is enough water in the reservoir.
[b] Observed Q_S in 2004 was 221 × 10^6 m^3 a^{-1} and 218 m^3 a^{-1} for the entire calibration period.
[c] RVE is the annual ration of simulated accumulated discharge and observed accumulated discharge.
[d] Observed Q_V in 2004 was 486 × 10^6 m^3 a^{-1} and 533 × 10^6 m^3 a^{-1} for the entire calibration period.

[46] Based on our hydrological projections, the seasonal run off generation dynamics will significantly change in the Vispa valley. Glaciers will continuously decrease until they almost disappear by the end of the 21st century (Figure 1). While temperature and global radiation are expected to increase throughout the entire year (Figures 7a and 7c), it is difficult to define distinct trends in precipitation patterns (Figure 7b). As a consequence of warmer temperatures, snow melt will occur earlier in the year and generate less runoff in the second half of the year (Figure 7d). The most eminent changes will be driven by the shrinking of the glacier extents in the entire catchment, which will lead to a decrease of glacier runoff throughout the 21st century [*Farinotti et al.*, 2011; *Huss et al.*, 2008]. This projection is in accordance with the observations throughout the last 10 years, which show an average decline of Q_M and Q_Z of 102 km^3 a^{-1} and 4000 m^3 a^{-1}, respectively (Figures 5b and 5c). Based on the model projections, the decline of Q_M and Q_Z will continue, as illustrated in Figures 7f and 7g. While the increased snow and ice melt in spring will lead to enhanced runoff in spring, runoff in the second half of the year will be significantly lower. Subsequently, this seasonal shift will impact hydropower production. The water released at Stalden entirely depends on the hydropower operational rules, defined in the model by the water level in Mattmarksee (Figure 7h). The projections indicate that runoff water will be sufficient to fill Mattmarksee until the middle of the century, but water deficiencies will occur by the end of the century. These simulations rely on mean lake level observation as illustrated in Figure 6. In order to obtain similar lake level as today, future hydropower production will have to be significantly reduced during the second half of summer, while more power can be produced during spring (Figure 7i). This will of course significantly impact the river flow at Visp, leading to an additional shift of summer runoff to the winter months (Figure 7j).

[47] Table 8 summarizes the expected changes based on the presented projections. The greatest change over an entire hydrological cycle is expected in Q_{IM}, which is expected to be reduced by one third by the mid century and halved by the end of the century (Table 8). Slightly lower Q_{SM} and the reduction of Q_{IM} is expected to reduce Q_M and subsequently Q_S by about 17% by midcentury and 33% by the end of the century. In turn, snow melt is expected to increase by one third by the middle of the century and half by the end of the century during the low flow season. Nevertheless, all modeled hydrological variables are expected to decrease during the melt season. The reduction of Q_{IM} by one third by the middle of the century and

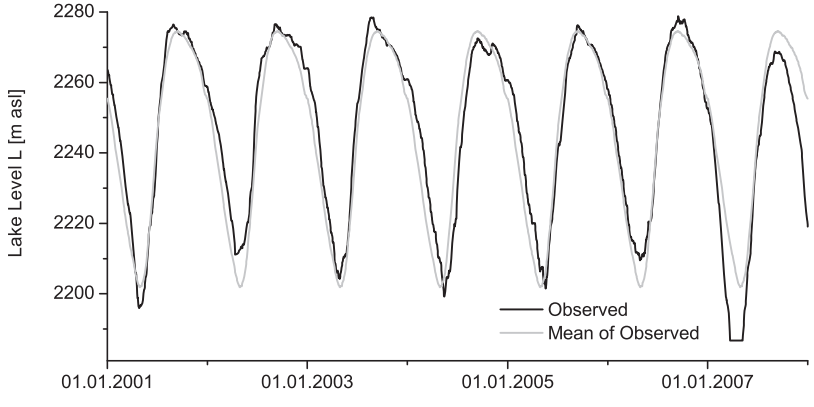

Figure 6. Observed lake level and daily mean lake level used for future hydrological projections.

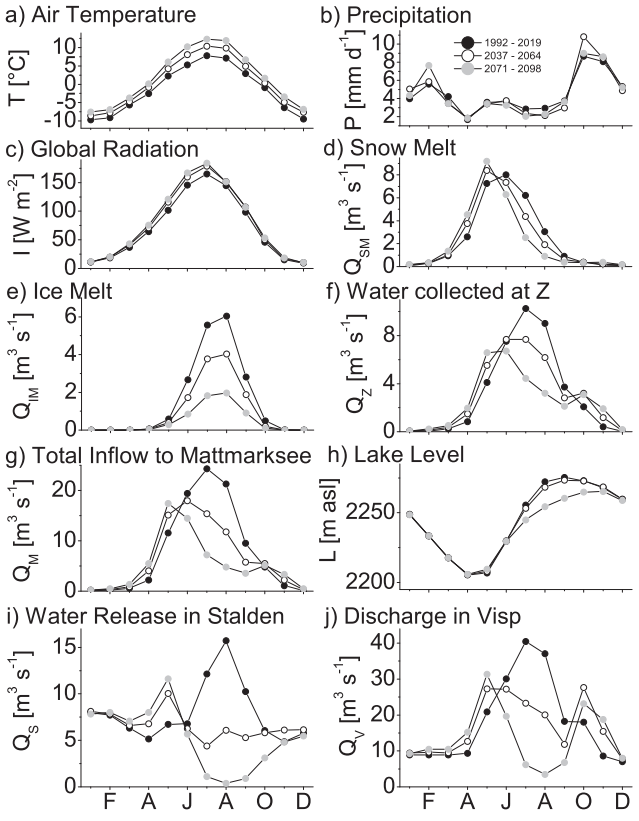

Figure 7. Monthly mean values of 10 selected variables for the three investigated time periods: (i) current reference time period (1992–2019), (ii) medium-term future time period (2037–2064), and (iii) long-term future time period (2071–2098).

one half by the end of the century will directly affect Q_S and subsequently Q_V. According to these results, hydropower production is expected to decrease by over half by the end of the century during the summer months.

4.3. Uncertainty Analysis of the Hydrological Projections

4.3.1. Uncertainty of Mean Discharge

[48] The multisimulation monthly mean ΔQ_M (mean of all 210 simulations) and its standard deviation for the medium- and long-term future period are illustrated in Figure 8a. Global uncertainty, namely the standard deviation of all 210 projections, remains below 3 $m^3\ s^{-1}$ in the middle of the century and below 2.5 $m^3\ s^{-1}$ at the end of the century, which is during July and August, when melt reaches its maximum, clearly less than the mean projected change ΔQ_M. As expected, uncertainty of the climate projections generates the largest uncertainty during the low flow season (October to April), as illustrated in Figures 8b and 8c, which is based on the ratio of the sum of squares between specific uncertainty sources and the total sum of squares. Up to midcentury, uncertainty due to the glacier extent is the largest source of uncertainty during the ice melt season (July and August). At the end of the century, when glacier extents have retreated drastically, the uncertainty generated by hydrological model parameters becomes dominant during the melt season, indicating that the equifinality problem becomes only relevant once glacier extents have retreated significantly. Variance contribution due to the nonlinear interaction between the different uncertainty sources and nonexplained variance is very low throughout the year.

[49] Moreover, in May, July, August, and September the uncertainty produced by the 210 simulations remains below the absolute value of the projected differences (Figure 8a), indicating that our projected changes are significant.

4.3.2. Uncertainty of Discharge Due to Natural Climate Variability

[50] Meteorological and hydrological long-term trends are only significant if the trends are stronger than the natural variability of the respective annual cycle. In Figure 9a multisimulation monthly mean ΔQ_M of all 210 simulations is visualized (same as in Figure 8a) including error bars illustrating the respective standard deviation of 28 years of

Table 8. Multisimulation Mean of the Relative Changes of Selected Variables Compared to the Present Reference Time Period

Variable		Mean Annual Change	Mean Low Flow Change	Mean Melt Season Change
		Medium Term Projections (2037–2064)		
T	(°C)[a]	1.81	1.27	2.41
P	(–)	0.01	0.05	−0.13
I	(–)	0.09	0.09	0.09
Q_{SM}	(–)	−0.05	0.33	−0.11
Q_{IM}	(–)	−0.34	−0.01	−0.33
Q_M	(–)	−0.17	0.75	−0.23
Q_Z	(–)	−0.05	0.76	−0.14
Q_V	(–)	−0.07	0.15	−0.25
Q_S	(–)	−0.17	0.08	−0.38
		Long Term Projections (2071–2098)		
T	(°C)[a]	3.25	2.24	4.36
P	(–)	0.01	0.12	−0.12
I	(–)	0.12	0.14	0.11
Q_{SM}	(–)	−0.11	0.64	−0.24
Q_{IM}	(–)	−0.67	−0.22	−0.67
Q_M	(–)	−0.33	1.45	−0.45
Q_Z	(–)	−0.19	1.40	−0.33
Q_V	(–)	−0.25	0.26	−0.54
Q_S	(–)	−0.33	0.14	−0.62

[a]For air temperature the absolute change is given, while all other values are relative changes compared to average of the present time period (1992–2019).

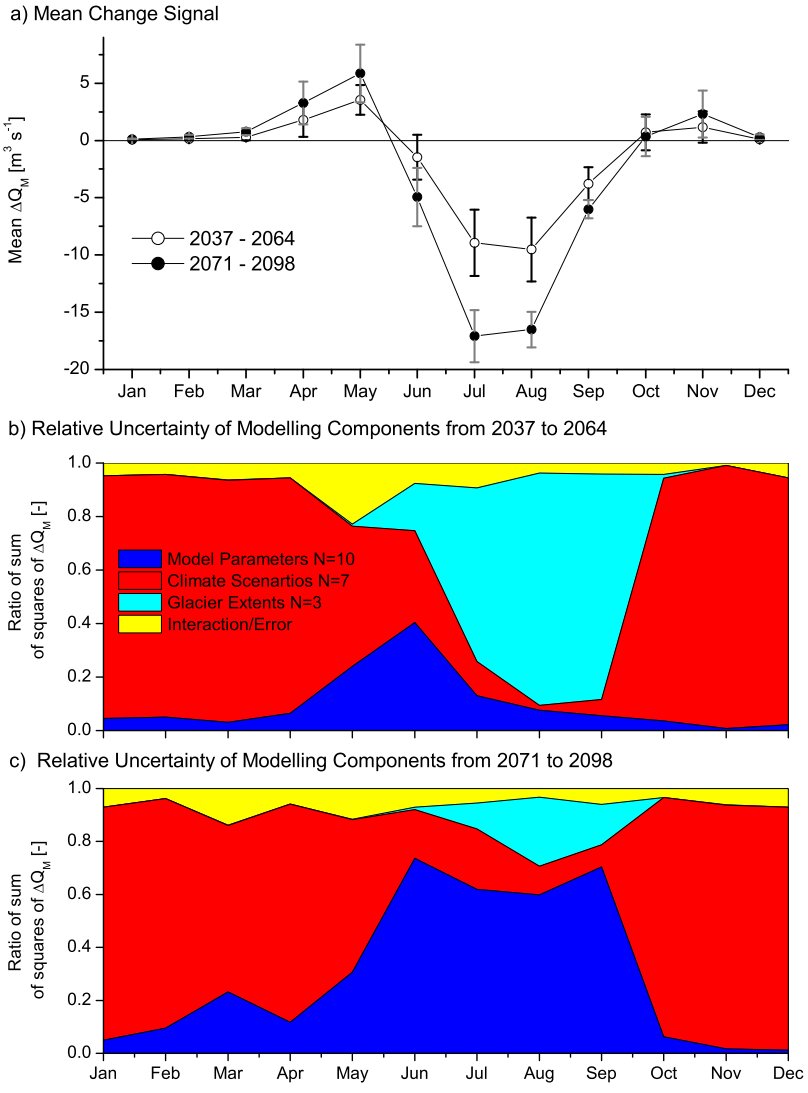

Figure 8. In (a) the multisimulation mean projected change in total input into Mattmarksee, ΔQ_M, based on the 7 climate scenarios, 10 plausible parameter sets of the hydrological model, and 3 glacier extents of the relevant time periods are illustrated. The whiskers represent the standard deviation of the 210 projections. In (b) and (c) the relative contribution of the individual modeling components to the global uncertainty for the medium- and long-term future time period is illustrated.

interannual variability. While the small changes during low flow season are smaller than the respective standard deviation, reduced ice melt in July, August, and September leads to significant changes in the runoff. As expected, largest interannual variability is projected in spring and fall, when ice melt and precipitation events lead to high variability in runoff generation (Figure 9b). Toward the end of the 21st century, variability is expected to increase particularly in spring and decrease in July and August, when glacier melt will be significantly reduced. We will discuss these circumstances and relate them to the different components of the hydrological cycle in section 5.

4.4. Impacts of High Water Events on Hydropower Production

[51] Particular attention should be given to the frequency and the intensity of heavy precipitation events, as these are expected to increase with climate change [*Luterbacher et al.*, 2004; *Milly et al.*, 2002]. This is especially important for hydropower production, as water intakes in the Vispa valley are constructed to meet present runoff (Table 4). Particular attention should be given to the water intake close to the village Saas Fee (Figure 1), as even today it is continuously overstrained during melt season (K. Sarbach, personal communication, KMW). The mean amount of excess water which cannot be collected at the water intake at Saas Fee, is illustrated in Figure 10. Today, most of the water is lost during the melt period, when ice and snow melt generate peak runoff. The annual amount of excess water is not expected to change significantly during the course of the century, however, a seasonal shift is expected. By midcentury, most of the excess water is expected during heavy precipitation events in October and November (Figure 10). Heavy precipitation events in fall are expected to

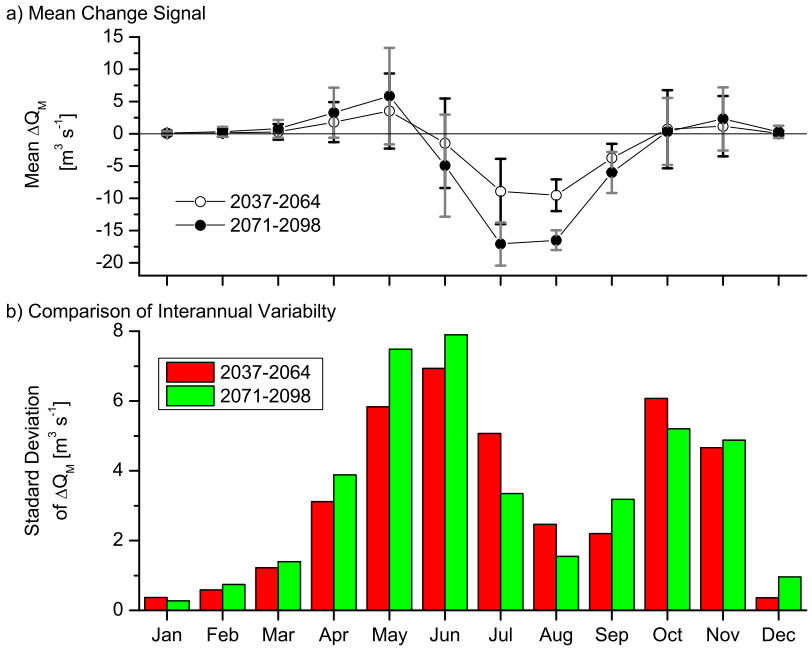

Figure 9. Interannual variability, illustrated as the standard deviation of the mean of 28 monthly averages of ΔQ_M each one representing one particular year in the future time period. In (a) the mean projected change in total input into Mattmarksee, ΔQ_M, is illustrated. The whiskers represent the standard deviation of the mean of the 28 year period. In (b) the standard deviation of the mean for the medium- and long-term time period are visualized.

become even more frequent at the end of the century (Figure 7b), while air temperature is expected to increase by almost 3°C (Figure 7a). As a consequence, projected runoff is expected to increase drastically during fall, as shown for the illustrative example at the water intake of Saas Fee (Figure 10). This result indicates that in the future peak runoff due to heavy precipitation events will become more important, while the rather constant runoff of ice melt during summer will decrease significantly.

5. Discussion

[52] Numerical projections based on future climate scenarios will always remain a partial description of natural processes influenced by climate change. Nevertheless, such projections remain the only possible way of projecting future changes. By using a stochastic model calibration, we take into account that the calibration of our physically based hydrological model is susceptible to the well-known equifinality problem [*Beven*, 2006; *Beven and Binley*, 1992], as different parameter sets reveal similar performances for the evaluation period, but lead to different projections under a changing climate.

[53] Nevertheless, our model setup leads to some discrepancies from observed data, in particular to overestimation of runoff generation in spring and underestimation during high summer (Figures 4 and 5; subplots b and c). The most eminent explanation for the discrepancies comes from the multivariable calibration technique: we calibrate our model with four criteria ($E_{Q,M}$, $E_{Q,Z}$, E_{VE}, and E_{CPSC}).

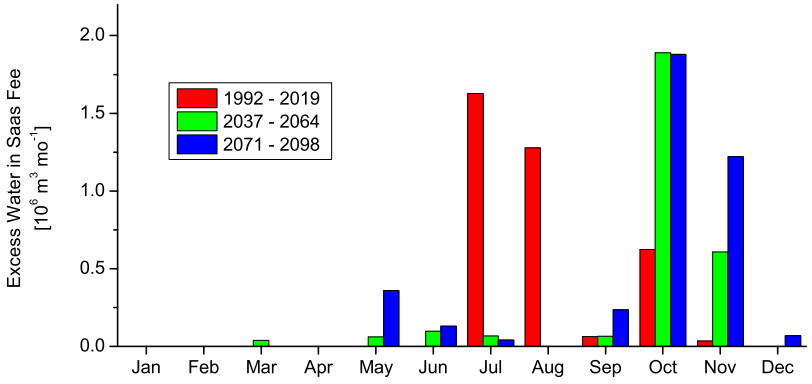

Figure 10. Multisimulation monthly mean runoff exceeding maximum capacity of the water intake in Saas Fee.

Accordingly model efficiency of one variable is lost in a tradeoff with model performance of other criteria. Furthermore, as already discussed by *Finger et al.* [2011], one weak point of TOPKAPI is the constant temperature gradient, which is in contradiction with observed seasonally varying temperature gradients in the region [*Rüedlinger*, 2010]. Indeed, in reality temperature gradients are rather lower in spring and higher in summer, which partially explains the overestimation in spring and underestimation in summer of melt runoff. A further source of error could also emerge from the tipping-bucket precipitation gauge used in Visp and Zermatt which underestimates solid precipitation by ∼20% compared to electronic weighing gauges [*Savina et al.*, 2011]. Finally, high water events are difficult to simulate, particularly because it is practically impossible to determine the maximum capacities of the water intakes. During heavy precipitation events, sediment and gravel can partially block the intakes while elevated hydrologic pressure may increase the theoretical water flow, making an exact determination of the maximum capacity impossible. Nevertheless, an error within the maximum capacities of water intakes is directly propagated to simulated water input to Mattmarksee. A further possible source of error is the rarely applied procedure of the hydropower company to release water from Saas Fee and Riedbach directly to Stalden (Table 4) instead of first diverting it to Zermeiggern.

[54] Even with a perfectly calibrated hydrological model, projections of future water resources rely on the accuracy of the applied climate scenarios. A comparison of the seven selected climate scenarios used in this study reveals a large uncertainty within the projected changes (Figure 3). Evidently, this uncertainty is propagated to the results of the hydrological model, as discussed with the uncertainty analysis (Figure 8). The uncertainty of the selected scenarios is particularly important in spring during snow melt and in fall when heavy precipitation events lead to runoff. Nevertheless, the climate scenarios used in this study are representative for the state of the art of regional climate change projections.

[55] In this study projections of glacier extent rely on the results presented by *Farinotti et al.* [2011], as TOPKAPI cannot account for glacier dynamics and retreat. Although these results were obtained with a different modeling approach, the continuous and gradual retreat of the glacier extent, along with the coarse spatial resolution of 250 m of our model, make this approach valid. As expected, the uncertainty of the glacier extent is the major uncertainty source during July and August when primarily ice melt leads to runoff generation. By the end of the century, this uncertainty will become less important, as ice melt contribution will have diminished due to the retreat of the glaciers. Furthermore, the retreat of the glacierized area will also affect the suspended sediment loads eroded beneath the glaciers leading to siltation of reservoirs, as investigated by *Finger et al.* [2006] and *Haritashya et al.* [2010] in other glacierized study sites.

[56] Interannual variability of the climate is independent of modeling performance, as it is simply due to the chaotic nature of the climate system. However, future climate projections indicate increasing interannual variability for the Alpine region with ongoing climate change for some state of the art RCMs [*Heinrich and Gobiet*, 2011]. Climatological and hydrological trends over several decades can therefore only be of statistical nature, making a deterministic projection for a specific year impossible. Nevertheless, the projected trends during glacier melting months indicate that mean ΔQ_M is larger than its respective standard deviation of interannual variability (Figure 9a). This suggests that the projected changes are strongly significant and that glacier retreat will drastically impact the runoff in July, August, and September.

[57] As all our simulations rely on the A1B emission scenario, our results do not take uncertainty due to different emission scenarios into account, so that the overall uncertainty due to climate projections is underestimated. Given that future greenhouse gas emissions are the product of very complex dynamic systems, depending on socioeconomic development, and technological change, their future evolution is very uncertain [*Nakicenovic et al.*, 2000]. Nevertheless, the A1B scenario describes a world that has rapid economic growth, quick spreading of new and efficient technologies, and a global population that reaches 9 billion by the midcentury and then gradually declines, it seems to be a realistic scenario for future projections.

[58] Considering that our projections are based on state of the art RCM scenarios and accounting for the discussed uncertainties, we could demonstrate that the presented future changes in runoff generation are statistically significant. Nevertheless, our results remain projected trends and not deterministic forecasts. It is very probable that increasing air temperature will lead to enhanced snow melt in spring and drastic reduction of ice melt, due to a drastic retreat of the glaciers. Based on these projections up to the end of the 21st century, it is expected that water supply will increase during winter but will be insufficient to completely fill Mattmarksee during the melting season. Accordingly, hydropower companies will have to adapt their energy production to the altered hydrology.

[59] Particular attention should be given to the peak flow frequencies, during which many water intakes are overstrained. For example, today the water intake at Saas Fee is continuously overstrained during the strong melt season in summer. In the future, the water intake is expected to be rather overstrained during heavy precipitation events in fall. In order to anticipate such changes in the runoff generation, the infrastructure of hydropower companies should be adapted to heavy precipitation events, rather than strong melt periods.

[60] Overall, our integrative modeling approach—combining state of the art climate projections, dynamic glacier modeling, and hydrological modeling accounting for water storage in reservoirs and river diversion—proved to be a powerful tool to project future water resources for hydropower production. In view of an expected intensification of hydropower production in the future, such modeling approaches can provide helpful information for water strategists to anticipate the impacts of projected climate change.

6. Conclusions

[61] The impacts of climate change on future water resources and its subsequent effects on hydropower

production during the 21st century were assessed using an integrative modeling approach which allows simulating complex hydropower operations in an alpine catchment. For this purpose hydropower operational rules were implemented in the fully distributed, physically based hydrological model TOPKAPI and future projections of rainfall and melt runoff generation were performed by coupling glacier retreat projections from a dynamic glacier model and A1B forced error-corrected and downscaled RCM climate scenarios to TOPKAPI. Based on 7 future RCM climate projections, 10 parameterizations of the hydrological model, and 3 projected glacier extents, the uncertainty of projections for two future 28 year time periods were analyzed and the source of uncertainty was quantified. Based on the presented projections we could observe (1) a significant temporal shift of the seasonal runoff generation to earlier months in the year, (2) reduced runoff generation during summer, and (3) the necessity to adapt future hydropower production to the projected future runoff dynamics. Furthermore, the results of the uncertainty analysis reveal that, depending on period and season, any of the three regarded uncertainty components (climate projection, hydrological simulations, and glacier modeling) may propagate the largest uncertainty contribution to the projected total water availability for hydropower production. The main conclusions can be summarized as follows:

[62] 1. Although future climatic and hydrological projections are subject to large uncertainties, the consistent trends observed in all 210 projections are significant in May, July, August, and September, as mean projected changes are greater than their variability. The projected changes in July, August, and September are even greater than projected uncertainty due to interannual climate variability, indicating the projected changes will not be overtopped by natural climate variability.

[63] 2. The uncertainty analysis revealed that the largest fraction of uncertainty is propagated to the end result (total available water runoff) in spring and fall by climate model uncertainty and in summer by glacier extents till the middle of the century, and by hydrological model parameters at the end of the century. Although the absolute values of our projections have to be considered with due diligence, the general projected trends are significant and the results represent the best possible projections based on currently available RCM simulations.

[64] 3. Based on the presented projections, total runoff generation for hydropower production will decrease during the 21st century by about one third due to the massive retreat of the glaciers. Until the middle of the 21st century, runoff will remain sufficient to fully fill the Mattmarksee under current hydropower production schemes. In the second half of the 21st century, hydropower production will have to be reduced during the summer months in order to fully fill Mattmarksee. The reduction of ice melt will not be compensated by the potential increase of precipitation.

[65] 4. The seasonal dynamics of the seasonal runoff dynamics will significantly change in the future. In the future the melt season will start earlier in the year, but in the second half of the melt season water runoff will be drastically reduced because of the glacier retreat and the advanced snow melt in the spring months.

[66] 5. The seasonal shift of the hydrological cycle and the reduced ice melt generation will very likely force hydropower companies to adapt new water management strategies. The new strategies have to take into account that ice melt in summer will be drastically reduced, but the frequency of heavy precipitation events during fall will increase. Accordingly, the current practice of hydropower companies, of producing maximum energy during winter and relying on ice melt to fill the reservoirs, might be jeopardized by the end of the century.

[67] 6. By midcentury, high water events due to heavy precipitation events are expected to become more frequent than today, leading to an increase of water loss due to overflow at some water intakes during fall. While today most water is lost during strong melt periods in summer, the future dynamics of hydrology will lead to overflows in particular during heavy precipitation events in fall. This represents new challenges for hydropower companies to adapt their infrastructures accordingly.

[68] **Acknowledgments.** The present study is part of the ACQWA Project (assessing climate impacts on the quantity and quality of water), funded within the seventh Framework Program of the European Union (grant agreement no. 212,250). The ENSEMBLES data used in this work was funded by the EU FP6 Integrated Project ENSEMBLES (contract 505,539) whose support is gratefully acknowledged. Data on glacier evolution was established in the projects WWK (Department of Energy and Hydro Power, Canton Valais, Forces Motrices Valaisannes), CCHydro (Swiss Federal Office for the Environment, BAFU), and FUGE (Swiss National Science Foundation, NFP 61). In addition, we would like to express our sincere thanks to C. Abgottspon, T. Bilgischer, and K. Sarbach (all KMW) for the presented hydropower data about the *Kraftwerke Mattmak SE* and to C. Constantin (GD) for detailed information about the infrastructure of *Grande Dixence SE*. Furthermore, we are thankful to M. Huss and T. Bosshard for valuable discussions, D. Farinotti for providing glacier extent masks, S. Rimkus for advice on the TOPKAPI coding, and S. Bauer for proofreading the manuscript. Finally, we would like to thank the three anonymous reviewers who gave valuable comments on an earlier version of this manuscript.

References

Alfieri, L., P. Perona, and P. Burlando (2006), Optimal water allocation for an alpine hydropower system under changing scenarios, *Water Resour. Manage.*, *20*(5), 761–778, doi:10.1007/s11269-005-9006-y.

Bartolini, E., P. Claps, and P. D'Odorico (2009), Interannual variability of winter precipitation in the European Alps: Relations with the North Atlantic oscillation, *Hydrol. Earth Syst. Sci.*, *13*(1), 17–25.

Bauder, A., M. Funk, and M. Huss (2007), Ice-volume changes of selected glaciers in the Swiss Alps since the end of the 19th century, in *Annals of Glaciology*, Vol 46, edited by M. Sharp, pp. 145–149, International Glaciological Society, Cambridge.

Bergstrom, S., B. Carlsson, M. Gardelin, G. Lindstrom, A. Pettersson, and M. Rummukainen (2001), Climate change impacts on runoff in Sweden—Assessments by global climate models, dynamical downscaling and hydrological modelling, *Clim. Res.*, *16*(2), 101–112, doi:10.3354/cr016101.

Beven, K. (2006), A manifesto for the equifinality thesis, *J. Hydrol.*, *320*(1–2), 18–36, doi:10.1016/j.jhydrol.2005.07.007.

Beven, K., and A. Binley (1992), The future of distributed models—Model calibration and uncertainty prediction, *Hydrol. Processes*, *6*(3), 279–298.

Bosshard, T., S. Kotlarski, T. Ewen, and C. Schär (2011), Spectral representation of the annual cycle in the climate change signal, *Hydrol. Earth Syst. Sci. Discuss.*, *8*, 1161–1192.

Carenzo, M., F. Pellicciotti, S. Rimkus, and P. Burlando (2009), Assessing the transferability and robustness of an enhanced temperature-index glacier-melt model, *J. Glaciol.*, *55*(190), 258–274.

Christensen, N. S., A. W. Wood, N. Voisin, D. P. Lettenmaier, and R. N. Palmer (2004), The effects of climate change on the hydrology and water resources of the Colorado River basin, *Clim. Change*, *62*(1–3), 337–363, doi:10.1023/B:CLIM.0000013684.13621.1f.

Déqué, M., D. P. Rowell, D. Lüthi, F. Giorgi, J. H. Christensen, B. Rockel, D. Jacob, E. Kjellstrom, M. de Castro, and B. van den Hurk (2007), An intercomparison of regional climate simulations for Europe: Assessing uncertainties in model projections, *Clim. Change*, *81*, 53–70, doi:10.1007/s10584-006-9228-x.

Déqué, M., S. Somot, E. Sanchez-Gomez, C. M. Goodess, D. Jacob, G. Lenderink, and J. H. Christensen (2011), The spread amongst ENSEMBLES regional scenarios: Regional climate models, driving general circulation models and interannual variability, *Clim. Dyn.*, doi:10.1007/s00382-011-1053-x, in press.

Egre, D., and J. C. Milewski (2002), The diversity of hydropower projects, *Energy Policy*, *30*(14), 1225–1230.

Farinotti, D., S. Usselmann, M. Huss, A. Bauder, and M. Funk (2011), The runoff evolution in the Swiss Alps: Projections for selected high-alpine catchments based on ENSEMBLES scenarios, *Hydrol. Processes*, doi:10.1002/hyp.8276, in press.

Finger, D., M. Schmid, and A. Wuest (2006), Effects of upstream hydropower operation on riverine particle transport and turbidity in downstream lakes, *Water Resour. Res.*, *42*(8), W08429, doi:10.1029/2005WR004751.

Finger, D., M. Schmid, and A. Wuest (2007), Comparing effects of oligotrophication and upstream hydropower dams on plankton and productivity in perialpine lakes, *Water Resour. Res.*, *43*(12), W12404, doi:10.1029/2007WR005868.

Finger, D., F. Pellicciotti, M. Konz, S. Rimkus, and P. Burlando (2011), The value of glacier mass balance, satellite snow cover images, and hourly discharge for improving the performance of a physically based distributed hydrological model, *Water Resour. Res.*, *47*, W07519, doi:10.1029/2010WR009824.

Frei, C., J. H. Christensen, M. Déque, D. Jacob, R. G. Jones, and P. L. Vidale (2003), Daily precipitation statistics in regional climate models: Evaluation and intercomparison for the European Alps, *J. Geophys. Res.*, *108*(D3), 4124, doi:10.1029/2002JD002287.

Hagemann, S., B. Machenhauer, R. Jones, O. B. Christensen, M. Déqué, D. Jacob, and P. L. Vidale (2004), Evaluation of water and energy budgets in regional climate models applied over Europe, *Clim. Dyn.*, *23*(5), 547–567, doi:10.1007/s00382-004-0444-7.

Hall, D. K., G. A. Riggs, V. V. Salomonson, N. E. DiGirolamo, and K. J. Bayr (2002), MODIS snow-cover products, *Remote Sensing Environ.*, *83*(1–2), 181–194.

Haritashya, U. K., A. Kumar, and P. Singh (2010), Particle size characteristics of suspended sediment transported in meltwater from the Gangotri Glacier, central Himalaya—An indicator of subglacial sediment evacuation, *Geomorphology*, *122*(1–2), 140–152, doi:10.1016/j.geomorph.2010.06.006.

Hauenstein, W. (2005), Hydropower and climate change—A reciprocal relation: Institutional energy issues in Switzerland, *Mt. Res. Dev.*, *25*(4), 321–325.

Heinrich, G., and A. Gobiet (2011), The future of dry and wet spells in Europe: A comprehensive study based on the ENSEMBLES regional climate models, *J. Climatol.*, doi:10.1002/joc.2421, in press.

Hock, R. (2005), Glacier melt: A review of processes and their modelling, *Prog. Phys. Geogr.*, *29*(3), 362–391, doi:10.1191/0309133305pp453ra.

Huss, M. (2011), Present and future contribution of glacier storage change to runoff from macroscale drainage basins in Europe, *Water Resour. Res.*, *47*, W07511, doi:10.1029/2010WR010299.

Huss, M., D. Farinotti, A. Bauder, and M. Funk (2008), Modelling runoff from highly glacierized alpine drainage basins in a changing climate, *Hydrol. Processes*, *22*(19), 3888–3902, doi:10.1002/hyp.7055.

IPCC (2008), *Technical Paper on Clim. Change and Water Rep., Intergovernmental Panel on Clim. Change*, Geneva.

Jager, H. I., and B. T. Smith (2008), Sustainable reservoir operation: Can we generate hydropower and preserve ecosystem values?, *River Res. Appl.*, *24*(3), 340–352, doi:10.1002/rra.1069.

Kay, A. L., H. N. Davies, V. A. Bell, and R. G. Jones (2009), Comparison of uncertainty sources for climate change impacts: Flood frequency in England, *Clim. Change*, *92*(1–2), 41–63, doi:10.1007/s10584-008-9471-4.

Lambrecht, A., and C. Mayer (2009), Temporal variability of the non-steady contribution from glaciers to water discharge in western Austria, *J. Hydrol. (Amsterdam)*, *376*(3–4), 353–361, doi:10.1016/j.jhydrol.2009.07.045.

Lehner, B., G. Czisch, and S. Vassolo (2005), The impact of global change on the hydropower potential of Europe: a model-based analysis, *Energy Policy*, *33*(7), 839–855, doi:10.1016/j.enpol.2003.10.018.

Luterbacher, J., D. Dietrich, E. Xoplaki, M. Grosjean, and H. Wanner (2004), European seasonal and annual temperature variability, trends, and extremes since 1500, *Science*, *303*(5663), 1499–1503.

Milly, P. C. D., R. T. Wetherald, K. A. Dunne, and T. L. Delworth (2002), Increasing risk of great floods in a changing climate, *Nature*, *415*(6871), 514–517.

Mimikou, M. A., and E. A. Baltas (1997), Climate change impacts on the reliability of hydroelectric energy production, *Hydrol. Sci. J.*, *42*(5), 661–678, doi:10.1080/02626669709492065.

Minville, M., F. Brissette, and R. Leconte (2008), Uncertainty of the impact of climate change on the hydrology of a nordic watershed, *J. Hydrol.*, *358*(1–2), 70–83, doi:10.1016/j.jhydrol.2008.05.033.

Miranda, L. E. (2001), A review of guidance and criteria for managing reservoirs and associated riverine environments to benefit fish and fisheries, *FAO Fisheries Technical Paper*, *419*, 91–137.

Nakicenovic, N., et al. (2000), *IPCC Special report on Emissions Scenarios Rep.*, Cambridge, UK and New York.

Nash, J. E., and J. V. Sutcliffe (1970), River flow forecasting through conceptual models Part I—A discussion of principles, *J. Hydrol.*, *10*, 282–290.

OFEN (2004), Ausbaupotential der Wasserkraft *Rep.*, 102 pp, Federal Office of Energy, Berne.

Payne, J. T., A. W. Wood, A. F. Hamlet, R. N. Palmer, and D. P. Lettenmaier (2004), Mitigating the effects of climate change on the water resources of the Columbia River Basin, *Clim. Change*, *62*(1–3), 233–256, doi:10.1023/B:CLIM.0000013694.18154.d6.

Pellicciotti, F. (2004), Development of an ice and snow melt model for long-term analysis of water resources from highly glacierised basins, PhD thesis, Swiss Federal Institute of Technology, Zurich.

Pellicciotti, F., B. Brock, U. Strasser, P. Burlando, M. Funk, and J. Corripio (2005), An enhanced temperature-index glacier melt model including the shortwave radiation balance: Development and testing for Haut Glacier d'Arolla, Switzerland, *J. Glaciol.*, *51*(175), 573–587.

Prein, A. F., A. Gobiet, and H. Truhetz (2011), Analysis of uncertainty in large scale climate change projections over Europe, *Meteorol. Z.*, *20*(4), 383–395, doi:10.1127/0941-2948/2011/0286.

Rüedlinger, D. (2010), Charakterisierung von Temperatur- und Niederschlagszonen im Rhonetal, BS thesis, Swiss Federal Institute of Technology, Zurich.

Savina, M., B. Schäppi, P. Molnar, P. Burlando, and B. Sevruk (2011), Comparison of a tipping-bucket and electronic weighing precipitation gauge for snowfall, *Atmos. Res.*, *103*, 45–51, doi:10.1016/j.atmosres.2011.06.010.

Schaefli, B., B. Hingray, and A. Musy (2007), Climate change and hydropower production in the Swiss Alps: Quantification of potential impacts and related modelling uncertainties, *Hydrol. Earth Syst. Sci.*, *11*(3), 1191–1205.

Schär, C., P. L. Vidale, D. Luthi, C. Frei, C. Haberli, M. A. Liniger, and C. Appenzeller (2004), The role of increasing temperature variability in European summer heatwaves, *Nature*, *427*(6972), 332–336, doi:10.1038/nature02300.

Seibert, J., and K. J. Beven (2009), Gauging the ungauged basin: How many discharge measurements are needed?, *Hydrol. Earth Syst. Sci.*, *13*(6), 883–892.

SGHL (2011), Auswirkungen der Klimaänderung auf die Wasserkraftnutzung – Synthesebericht *Rep.*, 28 pp, Schweizerische Gesellschaft für Hydrologie und Limnologie (SGHL) und Hydrologische Kommission (CHy), Bern.

Solomon, S., et al. (2007), The Physical Science Basis. Contribution of Working Group I to the Fourth Assessment Report of the Intergovernmental Panel on *Clim. Change*, in *Clim. Change*, edited by S. Solomon, et al., 996 pp., Cambridge Univ. Press, Cambridge.

Stahl, K., and R. D. Moore (2006), Influence of watershed glacier coverage on summer streamflow in British Columbia, Canada, *Water Resour. Res.*, *42*(6), W06201, doi:10.1029/2006WR005022.

Stahl, K., R. D. Moore, J. M. Shea, D. Hutchinson, and A. J. Cannon (2008), Coupled modelling of glacier and streamflow response to future climate scenarios, *Water Resour. Res.*, *44*(2), W02422, doi:10.1029/2007WR005956.

Sternberg, R. (2010), Hydropower's future, the environment, and global electricity systems, *Renew. Sustain. Energy Rev.*, *14*(2), 713–723, doi:10.1016/j.rser.2009.08.016.

Storch, H. V., and W. Zwiers (2003), *Statistical Analysis in Clim. Res.*, Cambridge University Press, Cambridge.

Suklitsch, M., A. Gobiet, A. Leuprecht, and C. Frei (2008), High resolution sensitivity studies with the regional climate model CCLM in the alpine region, *Meteorol. Z.*, *17*(4), 467–476, doi:10.1127/0941-2948/2008/0308.

Suklitsch, M., A. Gobiet, H. Truhetz, N. Khurshid Awan, H. Göttel, and D. Jacob (2010), Error characteristics of high resolution regional climate models over the Alpine area, *Clim. Dyn.*, *37*, 377–390,doi:10.1007/s00382-010-0848-5.

Themeßl, M. J., A. Gobiet, and A. Leuprecht (2011a), Empirical-statistical downscaling and error correction of daily precipitation from regional climate models, *J. Climatol.*, *31*(10), 1530–1544, doi:10.1002/joc.2168.

Themeßl, M. J., A. Gobiet, and G. Heinrich (2011b), Empirical-statistical downscaling and error correction of regional climate models and its impact on the *Clim. Change* signal, *Clim. Change*, doi:10.1007/s10584-011-0224-4, in press.

Todini, E. (1996), The ARNO rainfall-runoff model, *J. Hydrol.*, *175*(1–4), 339–382.

Todini, E., and L. Ciarapica (2001), The TOPKAPI model, in *Mathematical Models of Large Watershed Hydrology*, edited by V. P. Singh, chapter 12, 914 pp., Water Resources Publications, Littleton, Colorado.

Todini, E., and C. Mazzetti (2008), TOPKAP—TOPographic Kinematic AProximation and Integration—user manual and references *Rep.*, 137 pp, Protezione e Gestione Ambientale, Bologna.

Uhlenbrook, S., and A. Sieber (2005), On the value of experimental data to reduce the prediction uncertainty of a process-oriented catchment model, *Environ. Model. Software*, *20*(1), 19–32, doi:10.1016/j.envsoft.2003.12.006.

van der Linden, P., and J. F. B. Mitchell (2009), ENSEMBLES: *Clim. Change* and its impacts: Summary of research and results from the ENSEMBLES project *Rep.*, Met Office Hadley Centre, Exeter.

Xu, C. Y., and V. P. Singh (2004), Review on regional water resources assessment models under stationary and changing climate, *Water Resour. Manage.*, *18*(6), 591–612.

Zimmermann, M. (2001), Energy situation and policy in Switzerland, *Int. J. Ambient Energy*, *22*(1), 29–34.

A. Bauder, Laboratory of Hydraulics, Hydrology and Glaciology (VAW), ETH Zurich, Gloriastrasse 37/39, 8092 Zurich, Switzerland. (bauder@vaw.baug. ethz.ch)

D. Finger, Institute of Geography and Oeschger Centre for Climate Change Research, University of Bern, Hallerstrasse 12, CH-3012 Bern, Switzerland. (fingerd@gmx.net)

A. Gobiet and G. Heinrich, Wegener Center for Climate and Global Change, University of Graz, Leechgasse 25, 8010 Graz, Austria. (andreas.gobiet@uni-graz.at; g.heinrich@uni-graz.at)